Study on the Tumor Evolution in Glioblastoma Progression

A Thesis Submitted to
the Department of Science
and the Graduate School of Cancer Science and Policy
in Partial Fulfillment of Requirements
for the Degree of Ph. D. of Science

Sung Soo Kim

June 2020

GRADUATE SCHOOL OF CANCER SCIENCE AND POILCY

Professor Jong Bae Park (Supervisor)

We hereby approve the Ph. D. thesis of
[Sung Soo Kim]

June. 2020

Yun-Hee Kim	**sign**
Chairman of Thesis Committee	
Jong Heon Kim	**sign**
Thesis Committee Member	
Yun Soo Bae	**sign**
Thesis Committee Member	
Myung Jin Park	**sign**
Thesis Committee Member	
Jong Bae Park	**sign**
Thesis Committee Member	

NATIONAL CANCER CENTER
GRADUATE SCHOOL OF CANCER SCIENCE AND POLICY

ABSTRACT

[Study on the Tumor Evolution in Glioblastoma Progression]

Glioblastoma multiforme (GBM) is the most malignant brain tumor. Failure of GBM treatment is attributable to cancer evolution that driving resistance for anti-cancer treatment. To analyze evolutionary process of GBM during drug-resistance development, I performed massive proteogenomic analysis in AVASTIN treatment animal model. Interestingly, I identified periodic regulation of signaling network during drug resistance development. Among those genes, I focused on key molecular switches that regulate tumor microenvironment and stemness. The interplay between glioblastoma stem cells (GSCs) and tumor-associated macrophages (TAMs) promotes progression of glioblastoma multiforme (GBM). I identified that ARS2 (arsenite-resistance protein 2), a zinc finger protein that is essential for early mammalian development, plays critical roles in GSC maintenance and M2-like TAM polarization. ARS2 directly activates its novel transcriptional target *MGLL*, encoding monoacylglycerol lipase (MAGL), to regulate the self-renewal and tumorigenicity of GSCs through production of prostaglandin E_2 (PGE_2), which stimulates β-catenin activation of GSC and M2-like TAM polarization. I identify M2-like signature downregulated by which MAGL-specific inhibitor, JZL184, increased survival rate significantly in the mouse xenograft model by blocking PGE_2 production. To further analyze functional significance of WNT singling

during cancer evolution I combined WNT inhibitor, PRI 724 with AVASTIN, that significantly increased survival of mouse PDX model. These results suggest that cancer stemness that can be regulated by WNT signaling cooperate with tumor microenvironment to drive recurrence and resistance for anti-cancer therapeutics.

Contents

List of Figures

1. Introduction

Glioblastoma multiforme (GBM), a rapidly growing and highly invasive cancer, is the most common and lethal malignant primary brain tumor, with a median survival of 14 months and 2-year survival rates less than 10% (1). Despite the lethality and burden of the disease, there has been little progress in GBM therapeutics. Failure of GBM treatment is attributable in part to a small population of cells expressing resistance characteristics and its surrounding resistant microenvironments (2). The small population of GBM escape microscopic debulking surgery and recur because of invasive glioblastoma stem cells (GSCs) dynamically into brain parenchyma (3, 4). And those influence and communicate with multiple aspects of the GBM tumor microenvironment. One of the main regulatory components for the poor prognosis is that the small population acquires abilities such as high metabolic alteration, neo-vascularization and trans-differentiation into mesenchymal GBM (5, 6).

Tumor-associated macrophages (TAMs) are especially important in GBM, given their significant correlation with patient prognosis and glioma progression and grades. Interestingly, it has been shown that TAMs and GSCs, which are co-enriched in hypoxic and perivascular niches and are increased after recurrent GBM-irradiation, show a close functional relationship in conferring tumorigenesis (7, 8). Several previous studies have suggested that TAMs can be functionally subtyped according to polarization status, namely M1 and M2, a further demonstrated that M2 TAMs in particular play a tumor-supportive role in

GSCs. Notably, preventing TAM polarization into the M2 subtype has been reported to block glioma progression and tumor growth (7, 10). Despite the convincing functional correlation between TAM and GSCs, the molecular links defining the relationship between these two elements have not yet been defined.

Arenite resistance gene 2 (ARS2), first identified in an arsenite-resistant hamster cell line, contains multiple nuclear-localization signals and a zinc finger-like domain (11). In addition to its contribution to arsenite resistance, ARS2 is noteworthy for its role in mammalian development, modulation of cell proliferation, and promotion of the accumulation of several micro RNAs (miRNAs) involved in cellular transformation and inflammation (12, 13). A recent report demonstrates that ARS2 is closely associated with maintaining the self-renewal identity of neural stem cells (NSCs), identifying ARS2 as one of the transcription factors that controls pluripotent NSCs through direct induction of the pluripotent-maintenance gene, SOX2 (14). However, the role of ARS2 has never been studied in the context of cancer, let alone in glioma generally or GSCs in particular. Monoacylglycerol lipase (MAGL), encoded by the *MGLL* gene, is a lipolytic enzyme that hydrolyzes monoacylglycerols to glycerol and free fatty acids (FFAs) (15). MAGL is most highly expressed in the brain and white adipose tissue; however, is also highly expressed in aggressive cancer cells, where it modulates cancer metabolism through the production of FFAs (15-17) Another role of MAGL is to hydrolyze endocannabinoid 2-arachidonoylglycerol (2-AG) to arachidonic acid (AA), which can be enzymatically converted to prostaglandin E2 (PGE2) (18, 19). It has been shown that pharmacological blockade of MAGL

with clinically available inhibitors exerts anti-inflammatory effects in the brain and neuroprotective effects in mouse models of various neuroinflammation-mediated diseases (20). Despite convincing clinical evidence supporting the roles of MAGL, no studies have addressed the association of MAGL with the most fatal brain disease, GBM, and specifically GSCs. Furthermore, intriguing unanswered questions about potential regulators of MAGL remain at molecular and cellular levels. In this study, I provide the first demonstration that ARS2 regulates the stem cell-like characteristics of GSCs through direct transcriptional activation of MAGL. ARS2-MAGL signaling activates self-renewal by inducing the accumulation of β-catenin, and exerts tumorigenic activity in mouse xenograft models of GSCs by inducing M2-like TAM polarization, both of which are mediated by MAGL-dependent production of PGE2. Collectively, our findings establish MAGL as a prognostic factor in GBM, and show that pharmacological inhibition of MAGL offers potential benefit in the treatment of GBM.

Furthermore, recent genomic and/or transcriptomic analysis results of glioblastoma (GBM) had demonstrated to identify molecular and biomedical profiling of the brain tumor disease associated with clinical phenotype distinguishment such as tumor 4 subtypes (21, 22), Proneural (PN), Neural (NE), Classical (CL) and Mesenchymal (MES) named on the bases of signature genes expression. Those four molecular subtypes are related to clinical correlation with median survival; Proneural 16.2yr (14.3–22.4), Neural 15.0yr (12.2–21.9), Classical 12.2yr (10.05–15.0), Mesenchymal 15.0yr (13.6–20.4) and mortality; Proneural (HR = 0.8; p = 0.4.), Neural (HR = 0.56; p = 0.1), Classical (HR = 0.45;

p = 0.02), Mesenchymal (HR = 0.54; p = 0.02) sourced from The Cancer Genome Atlas (TCGA) performed data analyses bank (21). Recent concurrent therapeutics of GBM is treated with temozolomide and radiation combination followed by maintenance temozolomide (23). However, median survival of GBM is less 15 months and 2-year survival rates less than 10% (24). Furthermore, PN to MES transition in the concept of recurrence has been implicated in therapeutic resistance in GBM relapse. MES GBM relapse gene signature and poor prognosis are also implicated in concept of GBM therapeutic development (25). And genomic and transcriptomic changes must be translated into changes at the functional proteins. Proteomic changes impact clinical phenotypes, functional protein expressions, molecular profiles, and clinical implications (26-29). Thus, TCGA performed a proteomic characterization using reverse-phase protein arrays, and the Clinical Proteomic Tumor Analysis Consortium (CPTAC) has performed mass spectrometry (MS)-based proteomic and/or phosphoproteomic analyses of tumor tissues from patients with colon, breast, brain and ovarian cancers. But for GBM patient in the concept of tumor evolution against therapeutic resistance have not demonstrated that proteomic signatures can impact clinical implications through impacting genomic and/or transcriptomic alterations. Furthermore, there is any murine model for validating therapeutic development in the concept of GBM relapse

Malignant GBM has the median survival is only 12 to 15 months. The patients have clinical and molecular pathogenesis features are necrosis related pseudopalisading cells and vascular endothelial growth factor (VEGF) highly

expression. Temozolomide and radiotherapy followed by maintenance temozolomide is the standard of concurrent treatment therapy for GBM patients of newly diagnosed glioblastoma after debulking surgery (30). However, the median survival of GBM is not prolonged since last 5 years. James J. Vredenburgh et al. in 2007 performed a phase 2 trial to recurrent GBM patient with bevacizumab plus irinotecan treatment after conventional standard care of GBM. The result shows that prolonged 6 month progression free survival (PFS) among all 35 patients was 46% and 6 month overall survival (OV) was 77%. Olivier L. Chinot et al. and Mark R. Gilber et al performed bevacizumab treatment after conventional standard care of GBM for newly diagnosed patient in 2014 followed by previous clinical trial. The results demonstrated that bevacizumab increased PFS 3 to 4 months vs. placebo in newly diagnosed patients. But any groups shows the resistance mechanism induced by humanized immunogobulin (Ig) G1 monoclonal antibody, bevacizumab on the therapeutics care of the patients elucidated clearly PFS with increased symptom burden, a worse quality of life, and a decline in neurocognitive with plus bevacizumab (31-33).

This study provides the first demonstration and mechanism of action induced by bevacizumab on GBM resistance. Historically and histologically, bevacizumab treated GBM has been considered learning resistant against bevacizumab. Since Food and Drug Administration (FDA) approved bevacizumab for GBM, the mechanism of action is not elucidated clearly. I began with easily accessible murine model for bevacizumab induced systemic resistance

mechanism through established bevacizumab treatment protocol (34). WNT signaling is prevailing signature for regulating self-renewal and differentiation during on developing central nervous system and neural stem cells. Furthermore, WNT signaling is activated by WNT3A through its crucial transcription factor β-catenin for proliferation and development. Our murine model shows that WNT signaling directly activated during response period of bevacizumab treatment preparing resistance and tumor rebound growth against the therapeutic care of GBM through ß-catenin axis. Finally, I validated specific Wnt/β-catenin inhibitor, PRI-724, previous failed clinical trial test to GBM patient for potential combination therapeutic in murine model for GBM patients was proved for developing new therapeutics combined with conventional treatment in the concept of murine tumor evolution model with the results of proteo-genome analysis(35-36).

2. Materials and Methods

2.1 Culture

293T and U87MG cells were maintained in Dulbecco's modified Eagle's medium (DMEM) supplemented with 10% fetal bovine serum (HyClone). Patient-derived GBM stem cells (528, X01, 578, 83 and 0502) were maintained in DMEM/F-12 supplemented with B27 (Invitrogen), EGF (10 ng/ml, R&D Systems), and bFGF (5 ng/ml, R&D Systems). PGE_2 was purchased from R&D systems.

2.2 Plasmids

The lentiviral construct pLenti6-ARS2-FLAG, expressing C-terminally FLAG-tagged human ARS2, was generated by first amplifying ARS2 by PCR using pLenti6-ARS2 (Cosmogenetech, unpublished plasmid), as a template, and then inserting the amplified DNA fragment into *Bam*HI-*Xba*I-CIP-treated pcDNA3-cFLAG (J.H.K., unpublished plasmid) generating pcDNA3-ARS2-FLAG. The final pLenti6-ARS2-FLAG construct was prepared by assembling *Eco*RI-*Xho*I–treated pLenti6-MCS (J.H.K., unpublished plasmid) and pcDNA3-ARS2-FLAG via an In-Fusion reaction (Takara). The lentiviral construct, pLenti6-MAGL, was generated by assembling *Bam*HI-*Eco*RI-treated pLenti6-MCS and MAGL, PCR-amplified from a human brain cDNA library (Clontech). For construction of the lentiviral construct containing the *MAGL* promoter region (pGreen-MAGL-pro), a ~2-kb region of the *MAGL* promoter, amplified by PCR using Huh7 cell genomic DNA as a template, was inserted into *Eco*RI-*Spe*I-digested pGreenFire1 using an

In-Fusion reaction (Takara). shRNA-expressing lentiviral constructs targeting ARS2 and MAGL were constructed by ligating annealed oligomers (see Supplementary Table 2) with *Age*I-*Eco*RI-digested pLKO.1puro (Addgene). All oligomers were purchased from Macrogen (Seoul, Korea). All constructs were verified by DNA sequencing (Cosmogenetech).

2.3 Lentivirus Production and Infection

Lentiviruses were produced as previously reported (Yin et al., 2016; Yin et al., 2017). Briefly, 3–4 × 10^6 293T cells were plated on 100-mm culture dishes, incubated for 24 hours, and then co-transfected with 4.5 μg of lentiviral constructs, 3 μg of psPAX2 (Addgene), and 1.5 μg of pMD2.G (Addgene) using 27 μl of Lipofectamine 2000 (Invitrogen). The medium was changed 6 hours after later, and 48 hours after transfection, medium containing lentivirus was harvested. Viral particles were concentrated and purified using a Lenti-X concentrator (Clontech). Cells were infected with lentivirus in the presence of 10 μg/ml polybrene.

2.4 Reverse Transcription-Polymerase Chain Reaction (RT-PCR)

Semi-quantitative and real-time RT-PCR was performed to determine mRNA levels as previously described (Yin et al., 2018; Yin et al., 2017; Yin et al., 2015b). Total RNA was isolated from cells using TRIzol reagent (Invitrogen) according to the manufacturer's instructions. Total RNA (1 μg) was used as a template to synthesize cDNA using M-MLV reverse transcriptase (Promega). Real-time RT-PCR analysis was performed on a LightCycler 480II real-time detection system

(Roche) using LightCycler 480 SYBR Green I Master Mix (Roche). The expression levels of target genes were normalized to that of GAPDH. Semi-quantitative RT-PCR products were analyzed on 1% agarose gel. The PCR primers are shown as follows: ARS2, sense 5′-AAGCTGGATTTCCGGAGGCA-3′ and antisense 5′-CCTGCTCCAGGATGCGAAGA-3′; MAGL, sense 5′-CCGCAGAGCATTCCCTACCA-3′ and antisense 5′-GCTGCAACACATCCCTGACG-3′; and GAPDH, sense 5′-GGAGTCCACTGGCGTCTTCAC-3′ and antisense 5′-GAGGCATTGCTGATGATCTTGAGG-3′.

2.5 Limiting Dilution Assays

For *in vitro* limiting dilution assays, GSCs were plated at decreasing densities (100, 50, 25, and 5 cells/well) in 96-well plates containing DMEM/F-12 supplemented with B27, epidermal growth factor (EGF; 10 ng/ml), and basic fibroblast growth factor (bFGF; 5 ng/ml). Limiting dilution assay results were processed using ELDA (Extreme Limiting Dilution Analysis) software, available at http://bioinf.wehi.edu.au/software/elda/.

2.6 Metabolite Measurements

Approximately 10^6 cells were used for determination of FFAs. After removing medium and washing with 20 mL PBS, cells were fixed by adding 500 μL of methanol. Fixed cells were obtained from the culture dish using a cell scraper and collected in a glass tube; cells remaining in the culture dish were removed using

an additional 500 μL of methanol and pooled with the initially collected cells. The glass tube was vortexed vigorously to completely lyse cells, after which HCl was added to a final concentration of 25 mM. Internal standard solution (50 μL of 0.1 mg/mL myristic-d27 acid) was added to the sample solutions and mixed well, after which samples were microcentrifuged for 10 minutes at 13,000 rpm. Supernatants were collected in fresh tubes, and 3 mL of isooctane was added to each sample. After mixing well, samples were centrifuged for 15 minutes at 2000 × g and the upper layer was collected. This extraction step was repeated two more times. The collected upper layer was dried using a vacuum centrifuge and stored at -20°C until gas chromatography/mass spectrometry (GC/MS) analysis. Methyl esterification of FFAs was performed after reacting with BCl_3-MeOH at 60°C for 30 minutes. All lipid standards, including internal standards, were purchased from Avanti-Polar Lipids and Sigma-Aldrich (St. Louis, MO, USA).

Fatty acid methyl esters were analyzed using an Agilent 7890/5975 GC/MSD system equipped with an HP-5 MS 30 m × 250 μm × 0.25 μm column (Agilent 19091S-433). Helium (99.999%) was used as carrier gas, and samples were run in scan mode, with application of a 5-minute solvent delay. The initial temperature was 50°C, and was raised to 120°C at a rate of 10°C/min and held for 2 minutes. Thereafter, temperature was raised to 250°C at a rate of 10°C /min and was maintained at that temperature for 15 minutes. The GC column was cleaned between runs by heating to 300°C. The extracted ion chromatogram corresponding to a specific fatty acid was used for quantitation.

2.7 Immunoblot Analysis

Proteins were extracted with RIPA buffer with complete protease inhibitors (Roche), separated by electrophoresis, transferred to PVDF membranes (Millipore), and blocked with 5% skim milk (BD). Primary antibodies against ARS2 (GeneTex), MAGL (Santa Cruz), Cytochrome C (BD), Cleaved caspase-3 (EMD millipore), and α-tubulin (Santa Cruz) were incubated overnight at 4°C. Immunoreactive bands were visualized using peroxidase-labeled affinity purified secondary antibodies (KPL) and the Amersham ECL prime western blotting detection reagent (GE Healthcare).

2.8 Chromatin Immunoprecipitation

For each ChIP reaction, ~1 × 10^6 X01 cells were crosslinked with 1% formaldehyde for 10 minutes at room temperature, and genomic DNA was fragmented into ~100–300 bp fragments by sonication according to the manufacturer's instructions (Thermo-Fisher Scientific). DNA-bound ARS2 was immunoprecipitated using an ARS2-specific antibody (Genetex). The associated DNA was then purified and analyzed by qRT-PCR to detect specific DNA sequences within the *MGLL* promoter that were bound *in vivo* by ARS2 protein. An antibody against IgG was used as a nonspecific control.

2.9 Immunocytochemical staining

GSCs (1.5 × 10^4 cells) were grown on 8-well chambered culture slides (Nunc). After 24 hours, cells were fixed with 2% paraformaldehyde (PFA) and

permeabilized by incubating with 0.25% Triton X-100 for 10 minutes at room temperature (RT). After permeabilization, GSCs were immunostained for the cancer stem cell markers, Nestin (BD Biosciences) and GFAP (MP Biomedicals), as well as ARS2 (Genetex), PGE2 (Abcam), and β-Catenin(Cell signaling) by incubating overnight at 4°C in a humidified chamber with primary antibody, diluted with antibody diluent buffer (IHC World). Immunoreactive proteins were visualized with the appropriate Alexa Fluor 488- or Alexa Fluor 568-conjugated secondary antibody (Thermo-Fisher Scientific). Nuclei were stained with 4',6-diamidino-2-phenylindole (DAPI; Sigma). Fluorescence images were obtained using an LSM 780 confocal laser-scanning microscope (Carl Zeiss).

2.10 *in Vivo* Study

All animal experiments were conducted in accordance with protocols approved by the Institutional Animal Care and Use Committee of the National Cancer Center, Republic of Korea. For the orthotopic mouse model (Yin et al., 2017; Yin et al., 2015a), cells were first resuspended in DMEM/F-12 supplemented with B27, EGF (10 ng/mL) and bFGF (5 ng/mL), and then transplanted into the left striatum of 5-week-old female BALB/c nude mice by stereotactic injection. The injection coordinates were 2.2 mm to the left of the midline and 0.2 mm posterior to the bregma at a depth of 3.5 mm. The tumors were extracted, pooled for each experimental group, and mechanically disaggregated using stainless steel operating scissors. The brain of each mouse was harvested and fixed in 4% PFA. JZL184 (30 mg/kg; Tocris Biosciences) was orally administered daily. Survival

was analyzed using GraphPad PRISM software (version 7; GraphPad PRISM, La Jolla, CA, USA).

2.11 Isolation and Activation of Mouse Peritoneal Macrophages

Three days after intraperitoneal injection of 1–5% thioglycolate into the abdominal cavity of a nude mouse, peritoneal macrophages were obtained under sterile conditions. The cells were harvested by washing the peritoneal cavity with cold PBS (Gibco), then centrifuged (300 × g, 7 min) and resuspended in Dulbecco's modified Eagle's medium (DMEM) (Gibco) supplemented with 10% fetal bovine serum and 1% penicillin/streptomycin (P/S) (Sigma-Aldrich, St. Louis, MO, USA). The cells were allowed to adhere for 4 h and then were washed to remove non-adherent cells and cultured in DMEM supplemented with 1% P/S. Finally, the purified macrophages were activated by incubating for 48 h with LPS (10 ng/mL; Sigma-Aldrich) or IL-4 (10 ng/mL; PeproTech, Rocky Hill, NJ, USA)."

2.12 Histology and Tissue Staining

For observation of histological features, brains were removed, fixed with 4% PFA for 24 hours at 4°C, sectioned at a thickness of 4 μm using an essential microtome (Leica RM2125 RTS), and stained with hematoxylin (DaKo) and 0.25% eosin (Merck). Prior to immunohistochemical and immunofluorescence staining for cancer stem cell markers, macrophage-associate markers and the ARS2-associated factors, PGE_2 (Abcam), Nestin (BD Biosciences), GFAP (MP Biomedicals), Iba-1 (Wako), CD86 (Abcam), CD206 (Santa Cruz), Arginase-1 (Santa Cruz), ARS2

(GeneTex), and MAGL (LSbio), sections were subjected to an antigen retrieval process using citrate buffer (pH 6.0), and endogenous peroxidase was blocked by incubating with 3% hydrogen peroxide. Tissue sections were then incubated overnight at 4°C in a humidified chamber with primary antibody, diluted with antibody diluent buffer (IHC World). Tissue sections for DAB staining were developed using 3,3'-diaminobenzidine (DAB; Vector Laboratories) as the chromogen. For immunofluorescent staining, sections stained with primary antibody were subsequently incubated with the appropriate Alexa Fluor 488- or Alexa Fluor 568-conjugated secondary antibody (Thermo-Fisher Scientific).

2.13 Bioinformatics Analysis

SRRT mRNA expression and patient survival plots, grouped by SRRT levels, were derived from the REMBRANDT database of the National Cancer Institute. All data in REMBRANDT, including microarray gene expression data, copy number arrays and clinical phenotype data from glioma specimens, are currently hosted by the Georgetown Database of Cancer (GDOC). All statistical analyses, evaluations of gene expression, and Kaplan-Meier estimations were performed using GraphPad Prism 5 (GraphPad Prism). Genomic and clinical data for glioma samples were downloaded from the TCGA data portal (http://cancergenome.nih.gov/). TCGA RNA sequencing data were analyzed using BAM files obtained from the Cancer Genomics Hub (http:/cghub.ucsc.edu). Expression measurements and RPKM (Reads Per Kilobase of transcript per Million mapped reads) values were estimated using the R package, DEGseq.

2.14 RNA-Sequencing Data Processing

RNA-Seq libraries were prepared using the TruSeq RNA Library Prep kit (Illumina) and were sent out for transcriptome resequencing. The Phred quality score of the obtained raw FASTQ files was checked using FastQC (www.bioinformatics.babraham.ac.uk/projects/fastqc). The sequences were mapped onto the hg19 and GRCh37 human genome using Subread aligners (v1.5.3) (Liao et al., 2013), and each resulting SAM file was analyzed using featureCounts (Liao et al., 2014) and SeqMonk software (v1.38.2, www.bioinformatics.babraham.ac.uk/projects/seqmonk).

For identification of differentially expressed genes (DEGs), read counts generated from featureCounts were normalized and quantified using the LPEseq package (Gim et al., 2016), which is designed for non-replicated samples. The counts from SeqMonk were generated using the RNA-Seq quantification pipeline of the software. Genes with a *P*-value less than 0.05 were chosen as significant DEGs. The resulting graphs of DEGs were represented using the Multiple Experiment Viewer (MeV; v4.9.0) (Saeed et al., 2003) of the TM4 software suite.

2.15. Statistics

All data are expressed as means ± standard error of the mean (SEM) from at least three independent experiments. The Kaplan-Meier method was used to plot survival curves. In the case of patients who were alive at the time of last follow-up, survival records were censored in our analysis. The Statistical Package for the Social Sciences software (version 16; SPSS, Chicago, IL, USA) was used for

statistical analysis. In the case of mouse experiments, results of multiple datasets were compared by analysis of variance (ANOVA) using the log-rank (Mantel-Cox) test. The results of two-dataset experiments were compared using a two-tailed Student's t-test. *P*-values < 0.05 were considered statistically significant; individual *P*-values are provided in figure legends.

3. RESULTS

Chapter 1. Tumor microenvironment

3.1 ARS2 Expression is Correlated with Poor Survival of Glioma Patients and GSC Stemness

To study the relationship between ARS2 and clinical outcome in glioma patients, I first analyzed the expression profile of ARS2 in the REMBRANDT (REpository for Molecular BRAin Neoplasia DaTa) database, which included data from 105 patients with astrocytoma, 181 with GBM, and 336 with all forms of glioma. ARS2 mRNA expression was significantly upregulated in glioma patients compared with that in non-tumor brain tissue from 28 patients (Fig 1a). Among 336 patients in the all-glioma group, patients with higher expression of ARS2 exhibited significantly shorter survival than those with low expression (Fig 1b). Notably, a similar significant relationship was also observed in 181 patients with GBM (Figure 1C). Consistent with this, increased expression of ARS2 predicted poor prognosis among all glioma and GBM patients in the TCGA (The Cancer Genome Atlas) database (Figures 1D and 1E). These results collectively reveal an important association between ARS2 mRNA expression and high-grade glioma as well as poor patient survival.

To interrogate the protein levels of ARS2 in glioma patients, I analyzed tumor tissues from 49 glioma patients and five normal brain controls from the National

Cancer Center (NCC), Republic of Korea. ARS2 protein was barely detectable in normal brains, but was widely and strongly expressed in patient tumor samples. Next, I examined whether ARS2 expression was relevant for stem-like properties in glioma. Immunofluorescence analyses revealed that ARS2 was coexpressed with Nestin (a marker of NSCs) in a human GSC X01-derived mouse xenograft sample (Figures 1G and 1H). Moreover, significant positive correlations between ARS2 and Nestin expression in the TCGA database are plotted in Figure 1I. Collectively, these results indicate that upregulation of ARS2 mRNA and protein is strongly associated with glioma malignancy and GSC self-renewal.

3.2 ARS2 Regulates the Self-Renewal and Tumorigenicity of GSCs

To determine whether ARS2 is involved in the regulation of glioma stemness, I selectively knocked down ARS2 expression in GSCs using two different short hairpin (interfering) RNAs (shRNAs), and assayed for sphere-forming ability and cell proliferation (Figures 2A–F). Specific knockdown of ARS2 suppressed expression of Nestin, a marker of undifferentiated cells, with a concurrent increase in the expression of glial fibrillary acidic protein (GFAP), a marker of differentiation, in GSC 528 and X01 cells (Figures 2A, 2D). Knockdown of ARS2 significantly decreased the sphere-forming ability of GSCs in limiting dilution assays (Hu and Smyth, 2009), a widely used method for determining the self-renewal capacity of stem cells (Figures 2B and 2E). Knockdown of ARS2 also significantly blocked proliferation of GSCs (Figures 2C and 2F). Conversely,

overexpression of ARS2 significantly increased sphere-forming ability and proliferation rate in GSCs (578 and 0502 cells).

To address the tumorigenicity of ARS2 *in vivo*, I created mouse xenograft models from the X01 control cell line and its ARS2-knockdown derivatives, and compared tumor mass and overall survival. Hematoxylin and eosin (H&E) staining of brain slices from tumor-bearing mice revealed a obvious decrease in tumor mass in ARS2-knockdown xenograft models compared with the corresponding parental control models (Figure 2G). Moreover, overall survival was significantly longer in both ARS2-knockdown xenografts than in control mice (Figure 2H). Collectively, these findings indicate that ARS2 is required for GSC proliferation and is essential for regulating GSC self-renewal and glioma tumorigenicity.

3.3 Identification of *MGLL* as a Novel Target Gene of ARS2

Considering that ARS2 is a well-known transcriptional regulator involved in the maintenance of NSC stemness, I performed transcriptome profiling using RNA sequencing (RNA-Seq) analysis after deletion of ARS2. Each gene identified as being downregulated upon ARS2-knockdown was carefully examined for its significance in cancer pathogenesis. Genes involved in housekeeping activities or those with an inconsequential relationship with cancer were excluded. The most promising gene downregulated upon ARS2-knockdown was *MGLL*, encoding MAGL (Figure 3A). Although there are numerous reports of a significant association of MAGL with aggressive cancers (Aaltonen et al., 2013; Nomura et al., 2010; Oliveras-Ferraros et al., 2014), there are no studies linking MAGL with

glioma.

To establish an association between MAGL and ARS2 expression, I first confirmed MAGL mRNA and protein expression in ARS2-overexpressing and -knockdown GSCs. Overexpression of ARS2 in GSCs upregulated MAGL at both mRNA and protein levels (Figures 3B and 3C). Conversely, reducing the expression of ARS2 in GSCs downregulated MAGL expression at both mRNA and protein levels (Figures 3D and 3E).

Using chromatin immunoprecipitation (ChIP) assays, I further examined whether *MGLL* is a direct downstream target of ARS2. To this end, I designed four primer pairs (regions 1–4) covering the -1300 to +26 bp region relative to the transcription start site (TSS) of *MGLL*. Antibodies against ARS2 effectively immunoprecipitated a specific region upstream of the *MGLL* gene corresponding to regions 3 (-1018 to -887 bp) and 4 (-1300 to -1093 bp). The relative enrichment of ARS2 in regions 3 and 4 was assessed by quantitative polymerase chain reaction (qPCR), which revealed 5- and 25-fold higher levels of ARS2 occupancy in regions amplified by primer sets 3 and 4, respectively, compared with immunoprecipitations with control IgG (Figures 3F and 3G). To confirm the transcriptional relationship between ARS2 and *MGLL*, I used a lentiviral-based reporter system to monitor the expression of a luciferase reporter gene linked to the upstream promoter region, identified above, containing binding site(s) for ARS2 (Figure 3H). These reporter assays were performed in GSC X01 cells, with or without co-infection with an ARS2-specific shRNA-expressing lentivirus. As shown in Figure 3H, ARS2 knockdown in X01 cells significantly decreased

relative luciferase expression, indicating reduced transcriptional activity of ARS2 toward *MGLL*. Collectively, these data demonstrate that a number of genes are potentially regulated at the transcriptional level by ARS2, and specifically identify *MGLL* as a novel target of ARS2 in GSCs, consistent with the role of MAGL in aggressive cancers.

3.4 MAGL Plays Important Roles in Regulating the Self-Renewal and Tumorigenicity of GSCs

I next asked whether MAGL itself regulates the self-renewal ability and tumorigenicity of GSCs. Sphere formation was remarkably increased in MAGL-overexpressing GSC 578 and 0502 cell lines (Figures 4A–4D). Conversely, deletion of MAGL in 528 and X01 cells completely abrogated sphere-forming ability (Figures 4E–4H). Moreover, MAGL knockdown in 528 and X01 cells induced expression of the astrocytic differentiation marker, GFAP, but decreased levels of the stemness marker, Nestin (Figures S4A and S4B). These loss- and gain-of-function analyses of MAGL demonstrated that the functional effects of modulating MAGL expression on GSC self-renewal are similar to those of modulating ARS2 expression. To examine the effects of ARS2-regulated MAGL expression on the recovery of GSC self-renewal capacity, I knocked down ARS2 and then overexpressed MAGL in GSC X01 cells. shRNA-mediated ARS2 knockdown markedly lessened self-renewal (Figures 4I and 4J), whereas overexpression of MAGL in GSC X01 cells resulted in the highest degree of self-renewal detected (Figures 4I and 4J). Notably, overexpression of MAGL in ARS2-

knockdown X01 cells restored self-renewal ability, producing a degree of stemness virtually identical to that of controls (Figures 4I and 4J).

To address the effects of MAGL *in vivo*, I orthotopically injected nude mice with control X01 cells or each of two different MAGL-knockdown X01 lines. Tumors were reduced in size, or were nonexistent, in MAGL-knockdown xenografts. Xenografted mice injected with MAGL-depleted X01 cells survived significantly longer periods than mice injected with control X01 cells (Figure 4K). These findings demonstrate that MAGL is capable of modulating the characteristics of GSCs, especially self-renewal and tumorigenicity**.**

3.5 MAGL Modulates GSC self-renewal through PGE_2/pLRP6/β-catenin signaling

Next, I examined downstream elements in the MAGL pathway involved in regulating GSC self-renewal. MAGL hydrolyzes monoacylglycerols to produce FFAs and regulates the enzymatic conversion of AA to PGE_2 (Nomura et al., 2010). To address the role of MAGL in GSCs, I first examined whether ARS2 depletion in GSCs modulates FFA levels by directly suppressing expression of MAGL, as previously reported in other cancers (Nomura et al., 2010). Ten naturally occurring FFAs were analyzed, and their number of carbons and degree of saturation were determined. No significant changes in the levels of any type of FFA were detected regardless of ARS2-knockdown status. suggesting that MAGL in the brain, especially in GSCs, does not modulate FFAs, but instead controls production of PGE_2 in response to targeting by the upstream factor, ARS2.

Previous studies have suggested that PGE_2–stimulated β-catenin accumulation and the activation stimulates stemness in leukemia stem cells, growth of colon cancer cells, and progression of glioma (Brocard et al., 2015; Castellone et al., 2005; Li et al., 2017). Therefore, I selectively knocked down MAGL expression using MAGL-targeting shRNA (shMAGL) and subsequently assessed PGE_2 levels and β-catenin expression in GSCs (Figures 5A and 5B). Knockdown of MAGL simultaneously decreased PGE_2 production and β-catenin accumulation in GSCs (Figures 5A and 5B). Since nuclear translocation of β-catenin is closely related with its role in transcriptional activation, I determined whether ARS2 or MAGL affects the nuclear localization of β-catenin. I measured β-catenin protein levels in fractionated nuclear or cytosolic lysates after ARS2/MAGL knockdown. The successful fractionation of nuclear and cytosol proteins was validated with Lamin B and β-actin, respectively. As expected, MAGL or ARS2 knockdown in 528 and X01 cells reduced β-catenin protein levels in nuclear fraction (Figures 5C, 5D). Moreover, treatment with PGE_2 increased β-catenin expression in a concentration-dependent manner in association with enhanced LRP6 phosphorylation (Figure 5E). The sphere-forming ability of GSCs was also increased in a concentration-dependent manner by treatment with PGE_2 (Figure S5D), an effect that was blocked by the specific inhibitor of TCF/β-catenin-mediated transcription, ICG-001 (Figures 5F and 5G) (Emami et al., 2004). Treatment of GSC 528 and X01 cells with ICG-001 significantly reduced GSC sphere-forming ability through downregulation of TCF/β-catenin-mediated cyclin D1 and c-Myc transcription (Figures 5H, 5I). Collectively, these findings strongly

suggest that MAGL regulates GSC self-renewal through PGE_2/pLRP6/β-catenin signaling.

3.6 ARS2/MAGL Induces M2-like Polarization of TAMs by Regulating PGE_2

PGE_2, regulated by MAGL, is one of the most important factors in the brain that facilitates neuroinflammation (Nomura et al., 2011). Accordingly, I next examined the impact of downregulating ARS2 or MAGL on macrophage density in GSC-derived xenografts. In these xenograft mouse models, ARS2 or MAGL knockdown decreased staining for Iba-1, a marker of TAMs (Bhat et al., 2013; Yin et al., 2017), suggesting inflammatory signaling associated with ARS2 or MAGL regulates the tumorigenicity of GSCs. Importantly, a number of studies have suggested that PGE_2 induces TAM polarization toward M2-like properties (Heusinkveld et al., 2011; Li et al., 2014; Luan et al., 2015; Na et al., 2015; Vasandan et al., 2016). Hence, I explored whether PGE_2 induces subtype-specific TAM polarization *in vitro* using peritoneal cavity-extracted macrophages. It has previously been reported that these two subtypes of TAMs acquire opposite functions in relation to cancer: the M1-like subtype protects against cancer by suppressing angiogenesis, whereas the M2-like subtype is more likely to worsen cancer prognosis through enhanced invasion and tumor growth (Hambardzumyan et al., 2016). Accordingly, I compared the degree of induction of TAM polarization into M1 or M2 macrophages by treating with lipopolysaccharide (LPS) or interleukin (IL)-4, respectively, or with PGE_2. Treatment with PGE_2 induced

expression of the M2-like macrophage markers, CD206 (MRC1), CD163 and ARG1 (arginase-1), to an extent comparable to that induced by IL4 (Fig. 6A–C) (Cherry et al., 2014; Gordon, 2003). Expression of Krupple-like factor 4 (KLF4), a key transcription factor that regulates expression of M2-like TAM genes (Luan et al., 2015), was significantly increased by IL4 or PGE_2 treatment (Figure 6A). In contrast, treatment of macrophages with PGE_2 reduced the expression of tumor necrosis factor (TNF)-α and CD86, markers of M1-like macrophages (Figures 6A–C) (Gordon, 2003; Luan et al., 2015). Moreover, when I cultured GSC 578 cells in conditioned media (CM) from macrophages which were inducted by LPS or IL4, respectively, IL4-induced M2-like-TAM CM increased expression of Nestin and decreased GFAP. To further delineate the interaction between TAMs and GSC stemness, I hypothesized that M2-like TAM secretes cytokines which likely promote GSC stemness. Here, I conducted cytokine arrays in macrophage after PGE_2 treatment. PGE_2 enhanced the expressions of Lipocalin 2, Serpin E1, G-SCF, HGF, VEGF, and IL6, which was confirmed by real-time PCR. Among the six genes, four of them (Lipocalin 2, HGF, VEGF, and IL6) were significantly upregulated by PGE_2 treatment. Collectively, these results confirm that PGE_2 promotes M2-like TAM polarization which enhances GSC stemness by secretion of cytokines such as Lipocalin 2, HGF, VEGF, and IL6.

Next, I examined PGE_2 in GSCs upon the expression status of ARS2 and MAGL using an immunofluorescence approach (Figures 6D–G). PGE_2 (red) was clearly detected in images of immune-stained tissue from mice injected with control X01 cells. As expected, PGE_2 was undetectable in tissues from mice

injected with ARS2-knockdown (Figures 6D and 6E) or MAGL-knockdown (Figures 6F and 6G) GSCs. I also investigated M1- and M2-like subtypes of infiltrating TAMs by marker expression. The M2-like TAM expression markers, CD206 and ARG1, were rarely detected in GBM tumors formed from GSCs virally infected with shARS2; instead, these tumors showed upregulation of the M1 marker CD86 (Figures 6D and 6E). A similar increase in CD86 expression and decrease in CD206 and ARG1 expression and PGE_2 production was observed in GSCs infected with shMAGL (Figures 6F and 6G). Therefore, our data support the conclusion that M1-like TAM polarization is increased by ARS2 or MAGL knockdown. Importantly, expression of the stemness marker Nestin was decreased and expression of the differentiation marker GFAP was increased in tumor tissues formed from ARS2- or MAGL-knockdown GSCs (Figures 6D–G).

Taken together, our data suggest that the elevated expression of MAGL in the brain controls neuroinflammation, as evidenced by the production of PGE_2, and further regulates GSC self-renewal and M2-like TAM polarization.

3.7 Pharmacological Inhibition of MAGL Impairs the Self-Renewal and Tumorigenicity of GSCs

To further investigate efficacy of MAGL blockade in regulating the stemness characteristics of GSCs, I employed an *in vitro* pharmacological approach using the MAGL-specific inhibitor, JZL184 (Long et al., 2009). JZL184 at a concentration as low as 1 μM eliminated detectable MAGL expression in the GSC cell lines, 528 and X01. This abrogation of MAGL expression was associated with

a remarkable decrease in the renewal capacity of both GSC cell lines, as shown by the results of limiting dilution assays (Figures 7A and 7B).

Next, I orthotopically implanted GSC X01 cells into the brains of nude mice, and then treated mice orally with JZL184 or vehicle every day. Treatment with JZL184 decreased tumor mass; immunohistochemical staining further showed that JZL184 decreased MAGL levels and the number of Iba-1–expressing cells (Figure 7C). Notably, administration of JZL184 was sufficient to suppress MAGL expression in GSCs and infiltration of TAMs (Figure 7C).

Production of PGE_2, the final manifestation of MAGL-induced neuroinflammation, was also extinguished by treatment with JZL184, as demonstrated by immunofluorescence (Figure 7D). M1-like TAM polarization, represented by the marker CD86, was increased in X01 cells by treatment with JZL184, whereas M2-like TAMs, marked by CD206 and ARG1 expression, exhibited an opposite response to JZL184 administration (Figures 7D and 7E). I confirmed that treatment with JZL184 downregulated the stemness marker Nestin, and upregulated GFAP (Figures 7D and 7E). Finally, I assessed the survival of xenograft mice following JZL184 treatment. These experiments revealed that survival was significantly longer for JZL184-treated xenograft mice compared with vehicle-treated controls (Figure 7F). These beneficial effects of JZL184 treatment indicate that pharmacological inhibition of MAGL suppresses the self-renewal and tumorigenic capacity of GSCs and promotes M1-like polarization of TAMs.

3.8 JZL184 Globally Downregulated M2-Like TAM Signature and Inversely Correlated with Patients Survival

To elucidate the global transcriptional change in tumor-resident macrophages, I established subcutaneous mouse models of GSC X01 cells. Then, $CD11b^+$ macrophages were isolated by fluorescence-activated cell sorting (FACS) from JZL184-treated mice. With constructed mouse models, I performed RNA-Seq to compare the gene set between the experimental mice and respective control X01 xenograft mice. Signature genes downregulated by JZL184 in RNA-Seq were positively correlated with M2 TAM gene signatures (Engler et al., 2012) (Figure 8A). So, I called the gene signature downregulated by treatment of JZL184 as M2-like TAM signature. Since the role of infiltrating M2 macrophage in GBM has been implicated in mesenchymal (MES) subtype patients and associated with poor prognosis of GBM (Wang et al., 2017), I examined possible relationship between M2-like macrophage enrichment and MES subtype. Interestingly, I observed strong expression of CD44 (a MES subtype marker) and ARG1 in edge region of control but not in JZL184 treated-orthotopic xenograft mouse model (Figures 8B). These results suggest that pharmacological inhibition of MAGL blocks MES subtype change which is triggered by infiltrating M2-like macrophage. Furthermore, I also analyzed M2-like signature in GBM patients and identified that M2-like signature was enriched in mesenchymal subtype patients, while patients with lower expression of the signature harbored non-mesenchymal subtypes (Figure 8C). Higher expression of M2-like TAM signature predicted significantly

shorter survival in 161 TCGA patient pools (Figure 8D).

Gene set enrichment analysis (GSEA) further indicated that inhibition of MAGL by JZL184 reduced stemness and invasiveness signatures (Figures 8E and 8F). Moreover, GSEA analysis revealed that JZL184 treatment increased lymphocyte associated gene sets. In summary, the above data indicate that pharmacological inhibition of MAGL by JZL184 reduces expression of a M2-like TAM gene signature and is a hallmark of tumor aggressiveness of GBM patients.

Chapter 2. Intermediate progenitor in tumor evolution for MES transition

3.9 Bevacizumab Treatment Promotes Necrosis Regions and Tumor Progression in GBM Murine Model

I mainly focused on realizing definition of drug resistance in the context of murine model representing humanized immunoglobulin (Ig) G1 monoclonal antibody, bevacizumab therapeutic of GBM patients. I established GBM resistance murine model with initial 70 mouse brain orthotopic model. After injection of U87MG, I grouped similar size of brain tumor growth for treating bevacizumab or vehicle to the murine model. The murine model treated with bevacizumab survived until 6.5 weeks after injection of U87MG with enhanced necrotic region within the tumor foci

around end of the murine life span (Figure 9A and B). A representative tumor size and tumor growth of U87MG phase analysis graph of MRI by a week-wise follow-up schedules show response period sustained against bevacizumab until 5 weeks. However, passing through 5 weeks, around 6 weeks after injection of U87MG increased tumor size and tumor growth rate with enhanced necrosis regions in the T2 flair MRI images, eventually (Figure 9C and D). The average median survival was 30 days in vehicle group vs. 40 days in bevacizumab group with enhanced necrotic foci started from 5 weeks and expressed hypoxia related necrosis marker, HIF-1α around pseudopalisading cells of necrosis regions (Figure 9E and F). The clinical features of pseudopalisading cells and necrosis regions with invasive immune cells around of necrosis and intranecrosis region represents similarity of humanized murine model against bevacizumab resistance.

3.10 Proteomic Landscape of Brain Tissue in Bevacizumab Murine Model

In this study, sequential week-wise bevacizumab treatment or vehicle brain 7 tissues were analyzed using a proteomic approach wherein each brain tissues were dissected from normal brain tissues by surgical knife homogenized via cryopulverization. And the cryopulverized powder

samples were aliquoted to facilitate exome sequencing, transcriptomic, and proteomic analyses on the same tissue samples. The murine characteristics, including age, gender, genomic background, tumor origin, tumor culture method were supervised for equal qualified proteomic analyses. Isobaric tandem mass tags (TMT)-based global Proteomics and TMT-based phosphoproteomcis analysis identified a total of 11,355 proteins and 32,889 phosphopeptides, respectively. To enable proteome data integration and analyzing, I performed normalization assay by total protein expressions values.

Proteomic alteration can impact systemic function of the individual. Murine brain tissue bearing human GBM-wise assessment of proteomic profiles identified 7 majority signatures in response period of 2 to 5 week tumor bearing tissues proteome analysis results, including Proneural, Neural, Synapses, Calcium signaling, WNT signaling, Gap junction, L1CAM. Meanwhile EMT, Hypoxia, Matrix organization, Invasiveness, Adipogenesis, Glycolysis signatures were identified in resistance period of U87MG 6week tumor bearing tissues proteome analysis results. The murine individual-wise assessment of proteomic profiles identified 12 majority signatures, including Proneural, Neuronal, Synapses, Calcium signaling, TCA cycle, OXPHOS, Oligodendrocyte, Hypoxia, Apoptosis, Phagocyte

vesicle, Myeloid, Negative immune response signatures were identified (Figure 10A). Examples of identified proneural (GBM) signature included CASK, DGK1, GSK3B, SOX10, ZEB2, previously associated with GBM molecular subtyping from genetic alteration profiles and survival advantages implications of TCGA Research Networks for large GBM cohort (Verhak et al). I also identified WNT signaling signature included CAMK2G, CTNNB1, PRKCA, RAC1, RHOA, previously associated with WNT signaling and GBM progression. Because WNT signaling has crucial roles in developing and controlling self-renewal and differentiation during central nervous system (CNS) development and Neural Stem Cell (NSC) formation in the concept of gliomagenesis. And I identified calcium signaling signature included ATP2A2, ATP2B2, GNAS, GRIN1, VDAC3. And I also identified gap junction signature included CSNK1D, GRB2, GUCY1A, LPAR1, TUBA1C, TUBB3 (Figure 10B and C).

3.11 Patient Derived GSCs have resistance mechanism against bevacizumab

Next, I examined patient derived GSCs have similar resistance phenotype patterns as well as the way of response to GBM cell line, U87MG against bevacizumab treatment. 83NS and 528NS are cultured in serum-free conditions (serum-free GSC-media included EGF, FGF and B27

supplement). To assess similar responding to bevacizumab as well as the U87MG murine model had, I orthotopically injected the two GSCs (83NS and 528NS) into our murine model were treated bevacizumab or vehicle as the same protocol as 10mg/kg by intraperitoneal (IP) route. Those murine brain tissues have the necrotic regions within the bevacizumab treated brain tissues in 83NS and 528NS murine models. And bevacizumab treated groups expands overall survival days compared to vehicle treated groups in the murine models. Also, 83NS and 528NS treated bevacizumab groups sustain response period preparing persistence period around 2.5 weeks and 7 weeks, respectively. However, vehicle treated group shows expired survival disadvantages during the response period of 83NS and 528NS bevacizumab treated murine models (Figure 11A – F).

The sequential week-wise bevacizumab treatment or vehicle brain tissues of patient-derived glioblastoma cells, 83NS and 528NS were analyzed using a proteomic profile approach wherein each brain tissues were dissected from normal brain tissues by surgical knife homogenized via cryopulverization. And the cryopulverized powder samples were aliquoted to facilitate genomic, transcriptome, and proteome analyses on the same tissue samples as the same way of U87MG proteogenomic analysis approaches. The murine characteristics, including age, gender, genomic

background, tumor origin, tumor culture method were supervised for equal qualified proteogenomic analyses. The proteomics and phosphoproteomics analysis identified a total of 11,355 proteins and 32,889 phosphopeptides, respectively. To enable proteome data integration and analyzing, I performed normalization assay by total protein expressions values (Figure S3A and B). Proteomic alteration can impact systemic function of the individual. Murine brain tissue bearing human GBM-wise assessment of proteomic profiles identified 5194 majority common signatures in U87MG, 83NS and 528NS, including Proneural, Synapses, Neuronal, L1CAM, WNT, GAP Calcium signaling, Neuronal system, Transmission across chemical synapses, Gap junction common signatures. Those signatures draw similar response sigmoid patterns against bevacizumab. U87MG has response period preparing resistance against bevacizumab during 2 to 5 weeks brain tumors tissues. However, Mesenchymal subtyped 83NS shows response period against bevacizumab during 2weeks. Meanwhile proneural subtyped 528NS shows response period against bevacizumab during 7 to 11 weeks for preparing resistance. The resistance signatures were identified after 5 week, 2 week 11 week of U87MG, 83NS and 528NS, respectively including EMT, Matrix organization, Hypoxia, Glycolysis and Adipogenesis signatures.

3.12 Proteo-genomics Analysis of ß-Catenin expression

During on response period of bevacizumab treatment in U87MG, 83NS, and 528NS murine model, WNT signaling identified within 2, 3, 4, 5 weeks for tumor growth and resistance occurred against bevacizumab treatmenet. ß-Catenin is a key transcription factor for WNT pathway. Thus, I integrated total mRNA sequencing results and proteme (LC-MS/MS) results for analyzing integrated proteo-genomics analysis (Figure 12).

CTBP1, CTNNB1 (ß-Catenin), RAC1, and MAP3K7 are controlled through post translational regulation. PRKCA, PPP2R5D, SKP1, RHOA, PLCB4, PPP2R1A, GSK3 ß, CSNK2A1, MAPK10, CAMK2G, and PPP2R5E are controlled through transcriptional regulation. Validated GSEA Results in the U87MG Bevacizumab treated Sequential week-wise Brain Tissue Samples. To understand what classes of genes are altered by bevacizumab treatment in U87MG murine model, I performed geneset enrichment analysis (GSEA). In bevacizumab driven U87MG GBM bearing brain orthotopic model, Neurotransmitter receptoer binding, L1CAM interactions and EMT genesets were the highest scoring genesets. Periostin (EMT Signature), FGFR1 (L1CAM Signature), GRIP2 (Neuronal System Signature) transcriptome expression analysis are validated in the cryopulverized homogenized U87MG bevacizumab or vehicle treated brain

tumor tissues RNA extracted samples.

3.13 Validated Down-signaling Axis of ß-Catenin by CHIP and *in vivo* model

To validate ß-Catenin expression blocked by Wnt signaling specific inhibitor, PRI-724 in patient-derived GSC. I perform chromatin immune-precipitation (CHIP) in 83NS by ß-Catenin antibody. And analyzed down-signaling axis, PPP2R1A and GSK3β expression in the CHIP samples of 83NS treated with vehicle or PRI-724. Furthermore, I treated PRI-724, ß-Catenin specific inhibitor combined with bevacizumab in U87MG. PRI-724 prolonged survival treated with bevacizumab compared to vehicle or mono-therapeutics (Figure 13).

4. DISCUSSION

In the current study, I demonstrate that ARS2 is a regulator of stem-cell identity in GBM, showing that it upregulates MAGL by directly mediating the transcription of the corresponding gene *MGLL* in GSCs. MAGL, in turn, enhances self-renewal ability and tumorigenic activation through PGE_2–mediated β-catenin accumulation and M2-like TAM polarization. Moreover, I provide the first demonstration that pharmacological inhibition of MAGL effectively suppresses GSC self-renewal and tumorigenicity—the major therapeutic challenges in GBM.

Most research on ARS2 to date has focused its significant regulatory roles in early development and proliferation (Gruber et al., 2009; Wilson et al., 2008), studies that have shown that genetic deletion of *Ars2* results in embryonic lethality. In its capacity as a component of the nuclear cap-binding complex, ARS2 acts through miRNA biogenesis to induce cell proliferation (Helfand et al., 2011). Although this transcriptional role of ARS2 in development is well represented in the literature, the potential relationship of ARS2 with cancer, particularly with GSCs, has received relatively little research attention. Our findings indicate that ARS2 expression is correlated with poor prognosis of glioma patients and, importantly, promotes the tumorigenicity of GSCs through direct transcriptional induction of *MAGL* in the brain. These findings demonstrate a new molecular mechanism for ARS2, showing that it is a critical transcription activator of MAGL in GSC self-renewal and tumorigenic processes. Furthermore, by enhancing our understanding of the transcriptional network in tumor-initiating GSCs, the results

of this study will aid in establishing tailored targeting strategies.

MAGL, a membrane-associated enzyme in the cytosol that catalyzes the release of FFAs from lipid chains, is highly expressed in advanced ovarian tumors and was recently reported to be essential for remodeling of the lipid network (Dinh et al., 2002; Long et al., 2009; Nomura et al., 2010). In the context of cancer, it has been shown that MAGL expression is elevated in aggressive human cancers and primary tumors, including breast, ovarian, and melanoma cancers (Aaltonen et al., 2013; Nomura et al., 2010; Oliveras-Ferraros et al., 2014). Another function of MAGL suggested by a recent study is as a crucial modulator of PGE_2, which is capable of directly sustaining β-catenin accumulation (Li et al., 2017). Likewise, our results demonstrate that MAGL acts through regulation of PGE_2 production, and not FFA-associated lipid modulation, to influence GSC self-renewal and tumorigenicity. Previous studies have suggested that PGE_2 simulates β-catenin accumulation, which is an important factor in activation of leukemia stem cells and glioma progression (Brocard et al., 2015; Castellone et al., 2005; Li et al., 2017). As expected in light of these findings, our examination of the mechanistic role of PGE_2 in β-catenin signaling in GSCs reveals that MAGL-mediated PGE_2 production induces β-catenin accumulation in GSCs. Moreover, treatment with PGE_2 increased β-catenin expression in a concentration-dependent manner. These observations reinforce our experimental finding that MAGL expression is associated with the maintenance of GSC characteristics.

Although downstream effects of MAGL on the lipolytic network have been extensively investigated, questions related to upstream regulation of MAGL

activity in cancer cells have remained unresolved (Yecies and Manning, 2010). In the current study, I propose that ARS2, an important transcription factor in GSCs, exerts control over MAGL by regulating the expression of its corresponding gene, *MGLL*, and that the ARS2-MAGL functional module plays an important role in neuroinflammation. Our ChIP assays using multiple primers covering different regions of the *MGLL* promoter demonstrated that the *MGLL* gene is a direct target of ARS2, further supporting the functional association between ARS2 and MAGL. Our study is also the first to show that MAGL maintains the characteristics of GSCs.

An additional interesting relationship explored here is the association between TAMs and GBM. GBM is a complex disease, and TAMs further exacerbate this complexity (Hambardzumyan et al., 2016). On the basis of correlation studies relating the survival of glioma patients with the expression of TAMs, previous investigators have classified TAMs into M1 and M2 subtypes according to their characteristics and specific markers (Hambardzumyan et al., 2016). Although this classification scheme is not absolute, each subtype generally exhibits a phenotype opposite that of the other: the M2-like subtype is correlated with high-risk glioma patients and tumor invasion, whereas the M1-like subtype is associated with suppression of angiogenesis and tumor growth—characteristics that may offer promising therapeutic advantages (Feng et al., 2015; Hambardzumyan et al., 2016). In the current study, I utilized an immunofluorescence approach to visualize CD86, a marker of M1-like TAM polarization, and CD206 and ARG1, markers of M2-like polarization. Overall,

knockdown of ARS2 or MAGL expression decreased neuroinflammation, but different trends in ARS2 and MAGL expression were observed in relation to the phenotypes of TAMs: whereas ARS2 and MAGL expression in GSCs were both correlated with upregulation of the M2-like phenotype, knockdown of either factor led to an increase in the M1-like polarization. Therefore, this study confirms previously reported functions of both types of TAMs in glioma.

The MAGL-selective inhibitor JZL184 virtually eliminated MAGL expression in GSCs. Already known for its high selectivity for MAGL, JZL184 treatment clearly suppressed MAGL expression both *in vitro* and *in vivo*, in association with a significant reduction in the self-renewal capacity of GSCs and suppression of neuroinflammation. It should be noted that previous studies in mice have shown that treatment with JZL184 is accompanied by side effects related to cannabinoid receptor 1-dependent signaling, including analgesia, hypothermia, and/or gastrointestinal bleeding (Guzman, 2003; Mitchell and Warner, 2006). Although our data support an important role for the ARS2-dependent MAGL mechanism described here, a comprehensive analysis of the safety profile of MAGL inhibitors as well as large-scale, patient-oriented studies designed to assess effectiveness should be conducted to confirm the clinical viability of targeting this mechanism. Such studies will hopefully facilitate translation of a future drug to treat aggressive GBM from bench to bedside. I identified ARS2 as a new and important transcription factor that promotes the stem cell identity of GSCs through MAGL-mediated signaling and further showed that blockade of MAGL provides a promising therapeutic avenue for treating GBM.

In the current studies of bevacizumab related clinical trials and clinical researches focused on the phenomenon of eventual event about bevacizumab itself. In the context of inhibitor development, initiating threshold to develop effective therapeutic should overwhelm rest of other thresholds. However, overcoming the initiating threshold for eventual event of therapeutic resistance is important in the current era of inhibitor development. Because an overwhelmed approaches to extending the quality life of bevacizumab are the application of new pharmaceuticals or co-administration therapeutics that can postpone or prevent the onset of bevacizumab resistance. Recent therapeutic development approaches are co-administration for postpone or prevent the resistance mechanism onset. In this overwhelmed threshold trials could overwhelm occurred resistance mechanisms and also suggest rational new therapeutic opportunities to improve clinical outcomes and quality of life within bevacizumab related clinical results patient pools data.

James J. Vredenburgh et al., Olivier L. Chinot et al. and Mark R. Gilber et al. demonstrated potentiated pharmaceuticals effect in the newly diagnosed or recurrence GBM patient with bevacizumab treatment alone or combined treatment. However, lack of elucidating the resistance mechanism after treating bevacizumab to those GBM patient makes poor prognosis or poor quality of life for them. Therefore, JBP lab in NCC demonstrated tumor

resistance revolutionary phenomenon is important for elucidating the resistance mechanism. Recent pharmaceutical development and its recurrence studies show eventual systemic mutated or alteration are important factor for the key mechanism, at the same time, not jump over next step against first pharmaceuticals development.

BIBLIOGRAPHY

1. T. R. Mercer, M. E. Dinger, J. S. Mattick, Long non-coding RNAs: insights into functions. *Nature reviews. Genetics* **10**, 155 (Mar, 2009).

2. J. S. Mattick, I. V. Makunin, Non-coding RNA. *Human molecular genetics* **15 Spec No 1**, R17 (Apr 15, 2006).

3. G. J. Hannon, RNA interference. *Nature* **418**, 244 (Jul 11, 2002).

4. W. P. Kloosterman, R. H. Plasterk, The diverse functions of microRNAs in animal development and disease. *Developmental cell* **11**, 441 (Oct, 2006).

5. A. Esquela-Kerscher, F. J. Slack, Oncomirs - microRNAs with a role in cancer. *Nature reviews. Cancer* **6**, 259 (Apr, 2006).

6. D. P. Bartel, MicroRNAs: genomics, biogenesis, mechanism, and function. *Cell* **116**, 281 (Jan 23, 2004).

7. G. A. Calin, C. M. Croce, MicroRNA signatures in human cancers. *Nature reviews. Cancer* **6**, 857 (Nov, 2006).

8. C. E. Stahlhut Espinosa, F. J. Slack, The role of microRNAs in cancer. *The Yale journal of biology and medicine* **79**, 131 (Dec, 2006).

9. C. Lopez-Camarillo *et al.*, MetastamiRs: non-coding MicroRNAs driving cancer invasion and metastasis. *International journal of molecular sciences* **13**, 1347 (2012).

10. A. A. Svoronos, D. M. Engelman, F. J. Slack, OncomiR or Tumor Suppressor? The Duplicity of MicroRNAs in Cancer. *Cancer research* **76**, 3666 (Jul 01, 2016).

11. W. Kong *et al.*, Upregulation of miRNA-155 promotes tumour angiogenesis by targeting VHL and is associated with poor prognosis and triple-negative breast cancer. *Oncogene* **33**, 679 (Feb 06, 2014).

12. Y. H. Feng, C. J. Tsao, Emerging role of microRNA-21 in cancer. *Biomedical reports* **5**, 395 (Oct, 2016).

13. J. Yin *et al.*, DEAD-box RNA helicase DDX23 modulates glioma malignancy via elevating miR-21 biogenesis. *Brain : a journal of neurology* **138**, 2553 (Sep, 2015).

14. K. S. Sheinerman, S. R. Umansky, Circulating cell-free microRNA as biomarkers for screening, diagnosis and monitoring of neurodegenerative diseases and other neurologic pathologies. *Frontiers in cellular neuroscience* **7**, 150 (Sep 10, 2013).

15. A. G. Bader, D. Brown, J. Stoudemire, P. Lammers, Developing therapeutic microRNAs for cancer. *Gene therapy* **18**, 1121 (Dec, 2011).

16. M. V. Iorio, C. M. Croce, microRNA involvement in human cancer. *Carcinogenesis* **33**, 1126 (Jun, 2012).

17. Z. Li, T. M. Rana, Therapeutic targeting of microRNAs: current status and future challenges. *Nature reviews. Drug discovery* **13**, 622 (Aug, 2014).

18. J. Yin *et al.*, DEAD-box RNA helicase DDX23 modulates glioma malignancy via elevating miR-21 biogenesis. *Brain : a journal of neurology* **138**, 2553 (Sep, 2015).

19. C. Presutti, J. Rosati, S. Vincenti, S. Nasi, Non coding RNA and brain. *BMC neuroscience* **7 Suppl 1**, S5 (Oct 30, 2006).

20. S. Rocak, P. Linder, DEAD-box proteins: the driving forces behind RNA metabolism. *Nature reviews. Molecular cell biology* **5**, 232 (Mar, 2004).

21. J. A. Chan, A. M. Krichevsky, K. S. Kosik, MicroRNA-21 is an antiapoptotic factor in human glioblastoma cells. *Cancer research* **65**, 6029 (Jul 15, 2005).

22. N. Yanaihara *et al.*, Unique microRNA molecular profiles in lung cancer diagnosis and prognosis. *Cancer cell* **9**, 189 (Mar, 2006).

23. J. Winter, S. Diederichs, Argonaute proteins regulate microRNA stability: Increased microRNA abundance by Argonaute proteins is due to microRNA stabilization. *RNA biology* **8**, 1149 (Nov-Dec, 2011).

24. X. Chen *et al.*, Characterization of microRNAs in serum: a novel class of biomarkers for diagnosis of cancer and other diseases. *Cell research* **18**, 997 (Oct, 2008).

25. J. Lu *et al.*, MicroRNA expression profiles classify human cancers. *Nature* **435**, 834 (Jun 09, 2005).

26. X. Chen *et al.*, Characterization of microRNAs in serum: a novel class of biomarkers for diagnosis of cancer and other diseases. *Cell research* **18**, 997 (Oct, 2008).

27. J. A. Chan, A. M. Krichevsky, K. S. Kosik, MicroRNA-21 is an antiapoptotic factor in human glioblastoma cells. *Cancer research* **65**, 6029 (Jul 15, 2005).

28. E. A. Gustafson, G. M. Wessel, DEAD-box helicases: posttranslational regulation and function. *Biochemical and biophysical research communications* **395**, 1 (Apr 23, 2010).

29. B. T. Hawkins, T. P. Davis, The blood-brain barrier/neurovascular unit in health and disease. *Pharmacological reviews* **57**, 173 (Jun, 2005).

30. C. Cordon-Cardo *et al.*, Multidrug-resistance gene (P-glycoprotein) is expressed by endothelial cells at blood-brain barrier sites. *Proceedings of the National Academy of Sciences of the United States of America* **86**, 695 (Jan, 1989).

31. K. P. Olive *et al.*, Inhibition of Hedgehog signaling enhances delivery of chemotherapy in a mouse model of pancreatic cancer. *Science* **324**, 1457 (Jun 12, 2009).

32. J. Yin *et al.*, DEAD-box RNA helicase DDX23 modulates glioma malignancy via elevating miR-21 biogenesis. *Brain : a journal of neurology* **138**, 2553 (Sep, 2015).

33. D. P. Bartel, MicroRNAs: genomics, biogenesis, mechanism, and function. *Cell* **116**, 281 (Jan 23, 2004).

34. J. Yin *et al.*, DEAD-box RNA helicase DDX23 modulates glioma malignancy via elevating miR-21 biogenesis. *Brain : a journal of neurology* **138**, 2553 (Sep, 2015).

35. B. Rubio-Viqueira *et al.*, An in vivo platform for translational drug development in pancreatic cancer. *Clinical cancer research : an official journal of the American Association for Cancer Research* **12**, 4652 (Aug 01, 2006).

36. C. P. Haar *et al.*, Drug resistance in glioblastoma: a mini review. *Neurochemical research* **37**, 1192 (Jun, 2012).

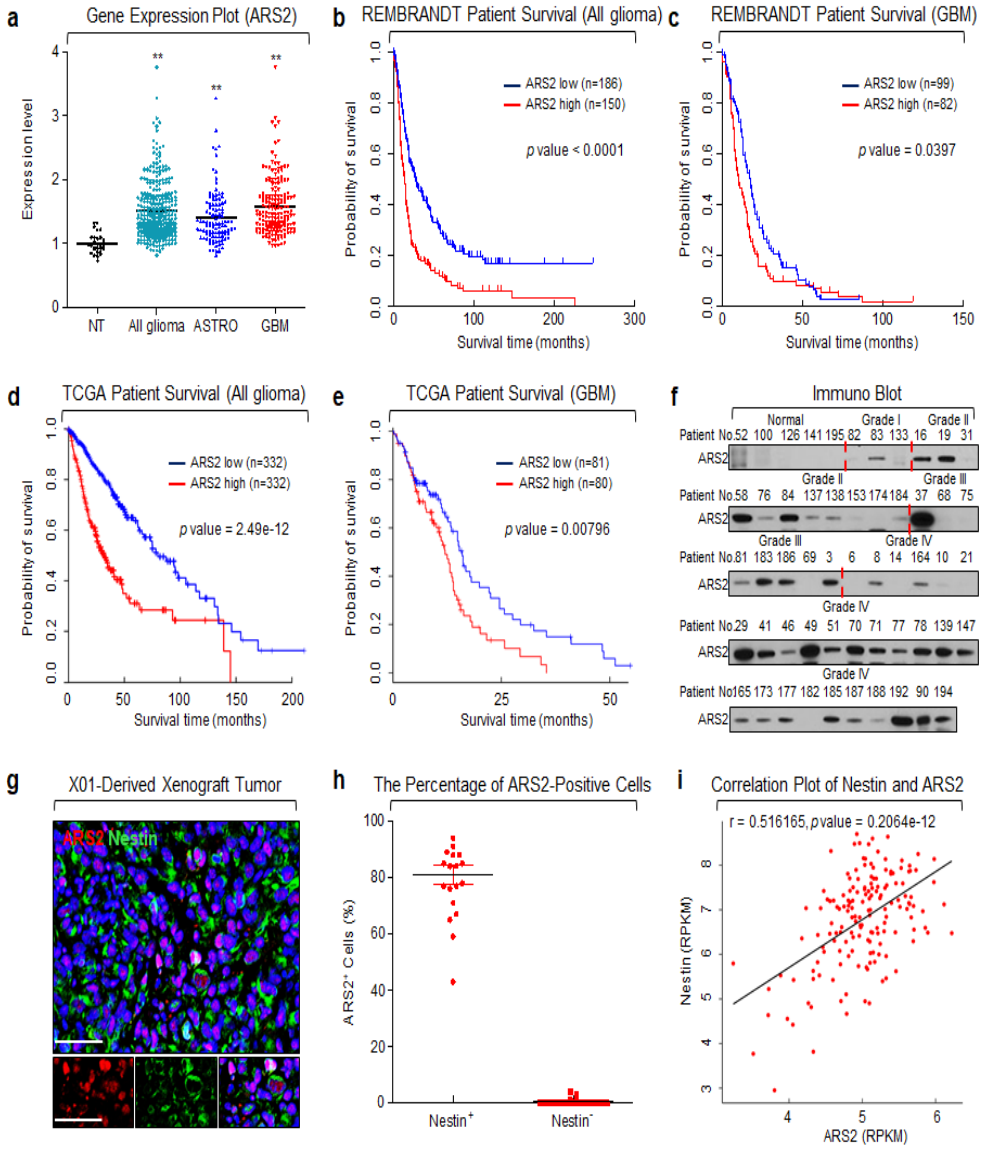

Figure 1. ARS2 Is Highly Expressed in High-Grade Brain Tumors

(A) ARS2 expression in each type of brain tumor from the REMBRANDT database.

(B and C) Kaplan-Meier survival plots for all glioma patients and GBM

patients with high and low ARS2 expression. Data were obtained from the REMBRANDT of the National Cancer Institute.

(D and E) Kaplan-Meier survival plots for all glioma patients and GBM patients with high (top 50% contribution) and low (down 50% contribution) ARS2 expression. Data were obtained from the TCGA database.

(F) Immunoblot (IB) analysis of ARS2 in patient tissues from normal brains and grade I-IV gliomas. GAPDH was used as a loading control.

(G) Immunofluorescence (IF) analysis of ARS2 and Nestin expression in GBM xenografts derived from X01 cells. Nuclei were counterstained with DAPI (blue).

(H) Percentage of ARS2-positive cells among Nestin-positive and -negative cells. Lines show means and ± SD.

(I) Correlation dot-plot of ARS2 and Nestin from the TCGA database (n=162).

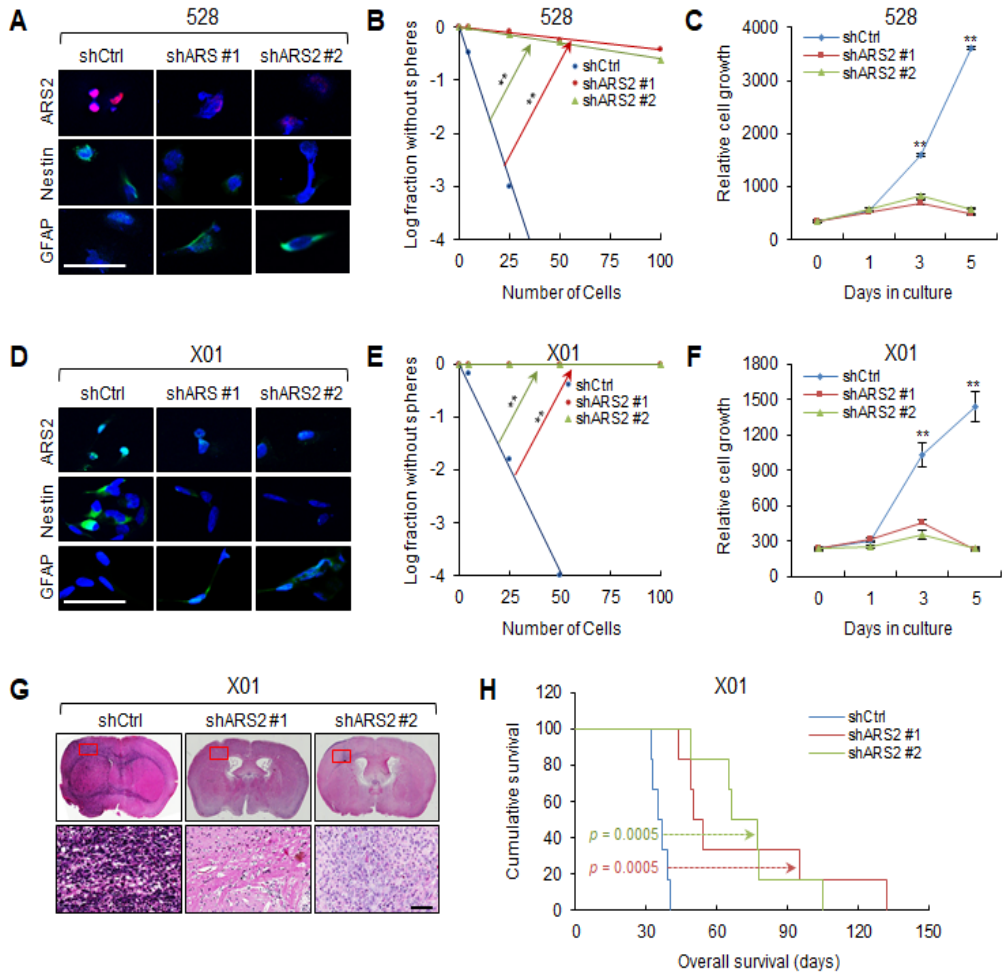

Figure 2. ARS2 Regulates the Stemness and Tumorigenesis of GSCs

(A) Immunocytochemical (ICC) analysis of ARS2, Nestin, and GFAP in control 528 cells (528-shCtrl), and two different ARS2-knockdown 528 cell lines (528-shARS2 #1 and 528-shARS2 #2). Nuclei were counterstained with DAPI (blue). Scale bar, 50 μm.

(B) Limiting dilution assays (LDAs) performed using 528-shCtrl, 528-shARS2 #1, and 528-shARS2 #2 cells.

(C) Cell proliferation assays performed using 528-shCtrl, 528-shARS2 #1, and 528-shARS2 #2 cells.

(D) ICC analysis of ARS2, Nestin, and GFAP in X01-shCtrl, X01-shARS2 #1, and X01-shARS2 #2 cells. Nuclei were counterstained with DAPI (blue). Scale bar, 50 μm.

(E) LDAs performed using X0-shCtrl, X01-shARS2 #1, and X01-shARS2 #2 cells.

(F) Cell proliferation assays performed using X01-shCtrl, X01-shARS2 #1, and X01-shARS2 #2 cells.

(G) H&E staining of the whole brains from mice implanted with X01-shCtrl, X01-shARS2 #1, or X01-shARS2 #2 cells. Scale bar, 100 μm. The sample is extracted at 42 days after cell injection.

(H) Kaplan-Meier survival plots for the orthotopic xenograft mouse model (n = 6; 1×10^5 cells injected per mouse).

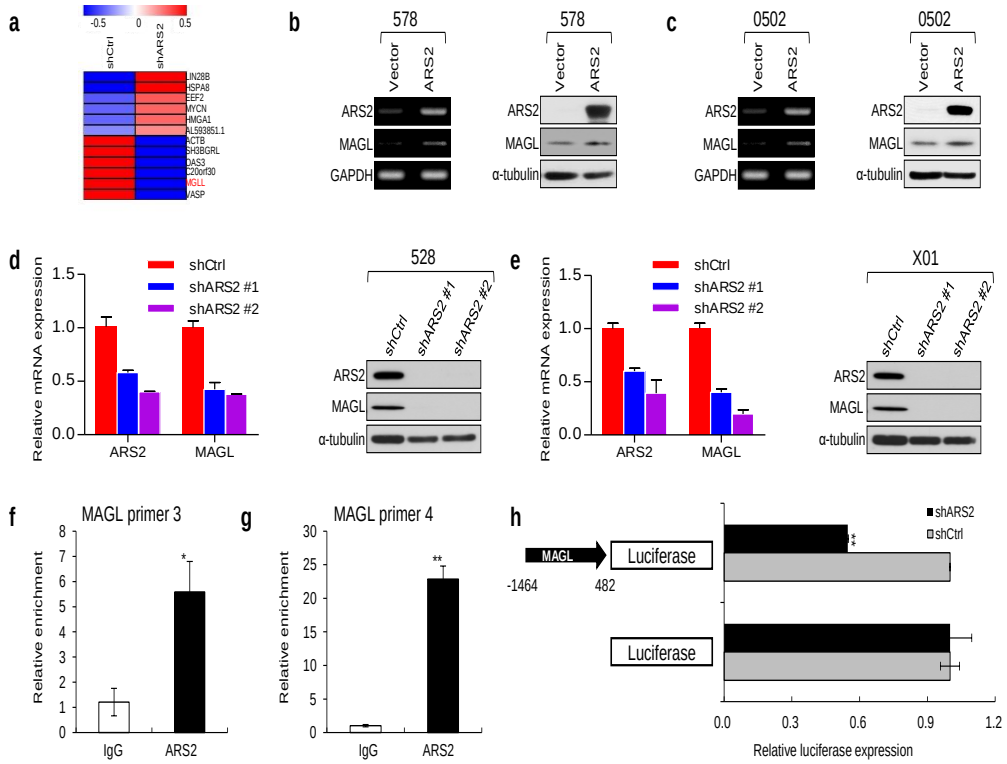

Figure 3. ARS2 Directly Activates Transcription of *MGLL*

(A) Heatmap analysis of gene expression in X01 cells infected with a shARS2-expressing lentiviral or shCtrl construct.

(B and C) PCR (left) and immunoblot (IB) analysis (right) of ARS2 and MAGL in GSCs (578 and 0502 cells) infected with an ARS2-expressing lentiviral or vector construct. GAPDH or α-tubulin was used as a loading control.

(D and E) PCR (left) and IB analysis (right) of ARS2 and MAGL in GSCs (528 and X01 cells) infected with a shARS2-expressing lentiviral or shCtrl

construct. GAPDH or α-tubulin was used as a loading control.

(F and G) Immunoprecipitated chromatin was analyzed by qPCR using 3- and 4-specific primers on the promoter region of the *MAGL* gene. Means ± standard error of the mean (SEM) are represented (**P* < 0.05, ***P* < 0.01).

(H) Luciferase reporter assays of MAGL activity in GSCs (X01 cells) infected with a shARS2–expressing lentiviral or shCtrl construct. Data are presented as means ± SEM (***P* < 0.01).

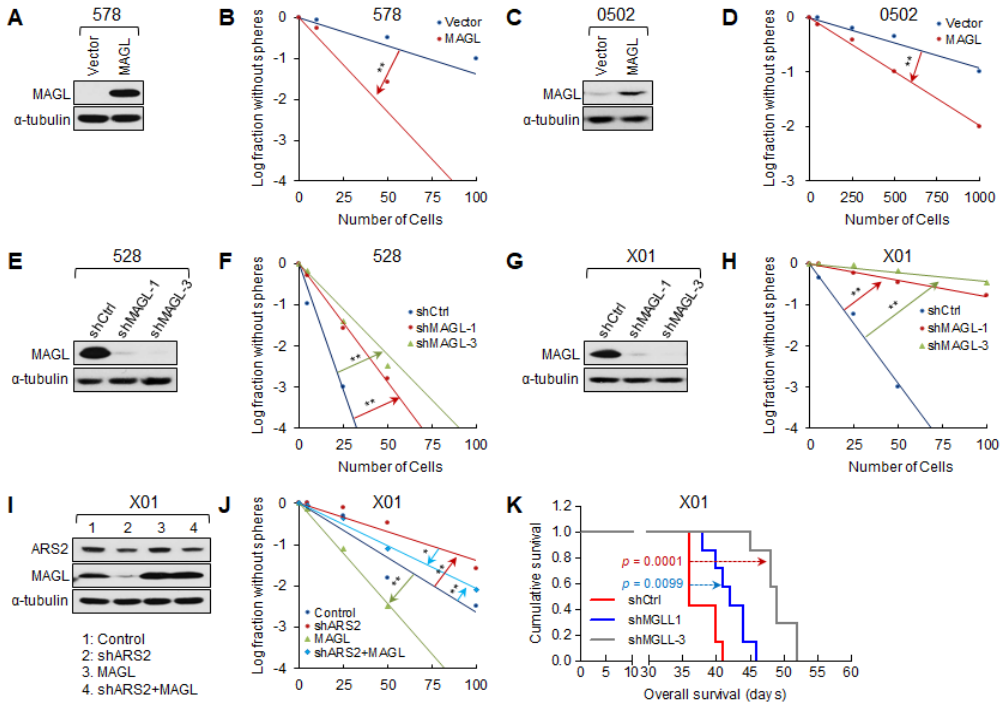

Figure 4. MAGL Regulates the Self-Renewal and Tumorigenesis of GSCs

(A) Immunoblot (IB) analysis of MAGL in GSCs (578 cells) infected with a MAGL-expressing lentiviral or vector construct. α-tubulin was used as a loading control.

(B) Limiting dilution assays (LDAs), performed in 578-vector and 578-MAGL cells.

(C) IB analysis of MAGL in GSCs (0502 cells) infected with a MAGL-expressing lentiviral or vector construct. α-tubulin was used as a loading

control.

(D) LDAs, performed in 0502- vector and 0502-MAGL cells.

(E) IB analysis of MAGL in GSCs (528 cells) infected with a shMAGL-expressing lentiviral or shCtrl construct. α-tubulin was used as a loading control.

(F) LDAs, performed in 528-shCtrl, 528-shMAGL-1, and 528-shMAGL-3 cells.

(G) IB analysis of MAGL in GSCs (X01 cells) infected with a shMAGL-expressing lentiviral or shCtrl construct. α-tubulin was used as a loading control.

(H) LDAs, performed in X01-shCtrl, X01-shMAGL-1, and X01-shMAGL-3 cells.

(I) IB analysis of ARS2 and MAGL in GSCs (X01 cells) infected with a shARS2- or MAGL-expressing lentiviral construct, both shARS2- and MAGL-expressing lentiviral constructs, or a shCtrl construct.

(J) LDAs, performed in GSCs (X01 cells) infected with a shARS2- or MAGL-expressing lentiviral construct, both shARS2- and MAGL-expressing lentiviral constructs, or a control construct.

(K) Kaplan-Meier survival analysis of mice implanted with X01 cells infected with shMAGL-expressing lentiviral or shCtrl construct (n = 7; 2×10^4 cells injected per mouse).

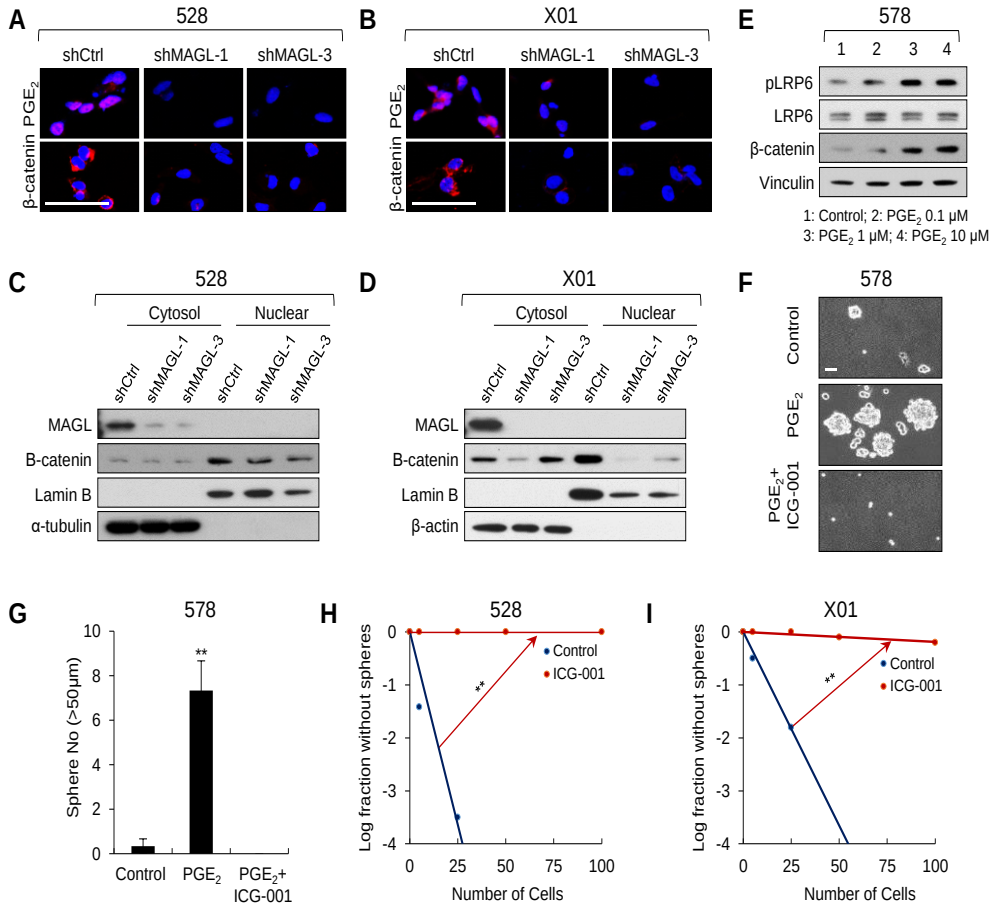

Figure 5. MAGL Modulates GSC Self-Renewal by Regulating PGE_2

(A and B) Immunocytochemical (ICC) analysis of PGE_2 and β-catenin in GSCs (528 and X01 cells) infected with a shMAGL-expressing lentiviral or shCtrl construct. Scale bar, 50 μm.

(C and D) Immunoblot (IB) analysis of MAGL and β-catenin in fractionated nuclear or cytosolic lysates from 528 cells and X01 cells infected with a shMAGL-expressing lentiviral or shCtrl construct. Lamin B and β-actin were used as a loading control.

(E) IB analysis of β-catenin in 578 cells treated with different concentrations of PGE_2 (0.1, 1, 10 μM). Vinculin was used as a loading control.

(F and G) Sphere-formation assays performed using GSCs (578 cells) treated with PGE_2 alone, PGE_2 and ICG-001 (10 μM), or vehicle. Images are representative of three independent experiments. Scale bar, 50 μm. The graph shows the average number of spheres greater than 20 μm in diameter. Data are expressed as means ± SEM (error bars) (n = 3, ** $P < 0.01$).

(H and I) Limiting dilution assays (LDAs) performed using GSCs (528 and X01 cells) treated with ICG-001 (10 μM) or vehicle.

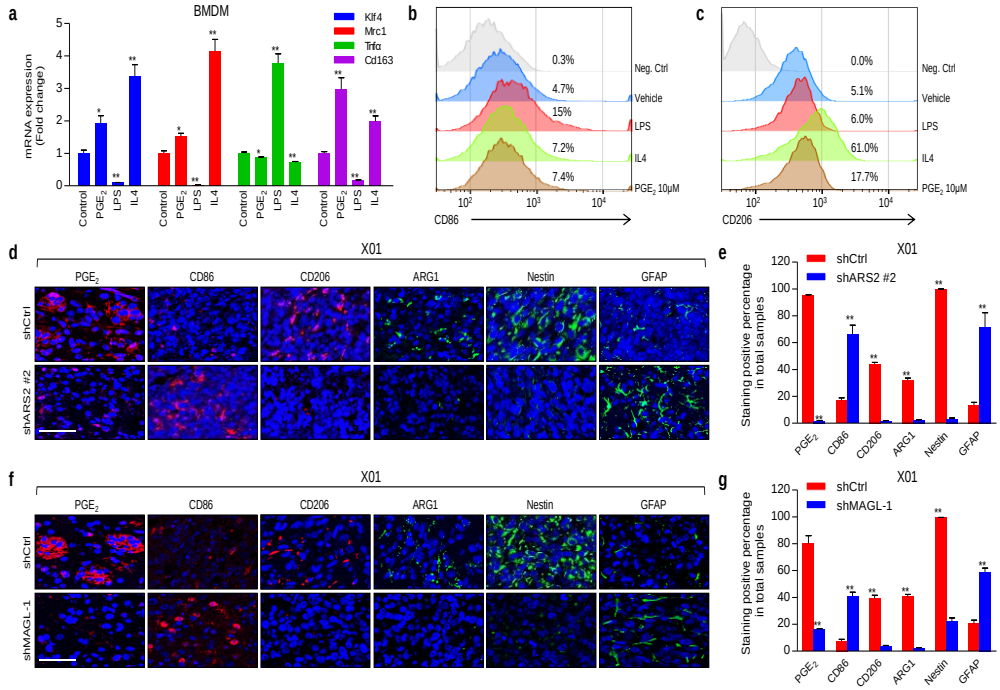

Figure 6. The ARS2/MAGL Module Regulates Tumorigenesis Through PGE$_2$–mediated Induction of M2-like TAMs

(A) qRT-PCR analysis of Klf4, Cd206, Tnfα, and Cd163 in peritoneal mouse macrophages after induction with PGE$_2$, LPS or IL4, or treatment with control.

(B and C) Immunocytochemical (ICC) analysis and quantification of CD86, CD206, and ARG1 in peritoneal mouse macrophages after treatment with PGE$_2$ or control. Scale bar, 50 μm. Data are expressed as means ± SEM (error bars) (n = 3, ** P < 0.01).

(D and E) Immunofluorescence (IF) analysis and quantification of PGE$_2$,

CD86, CD206, ARG1, Nestin, and GFAP in brain tissues from X01-shCtrl and X01-shARS2 #2 orthotopic xenograft mouse model. Scale bar, 50 μm. Data are expressed as means ± SEM (error bars) (n = 3, ** P < 0.01).

(F and G) IF analysis and quantification of PGE_2, CD86, CD206, ARG1, Nestin, and GFAP in brain tissues from X01-shCtrl and X01-shMAGL-1 orthotopic xenograft mouse model. Scale bar, 50 μm. Data are expressed as means ± SEM (error bars) (n = 3, ** P < 0.01).

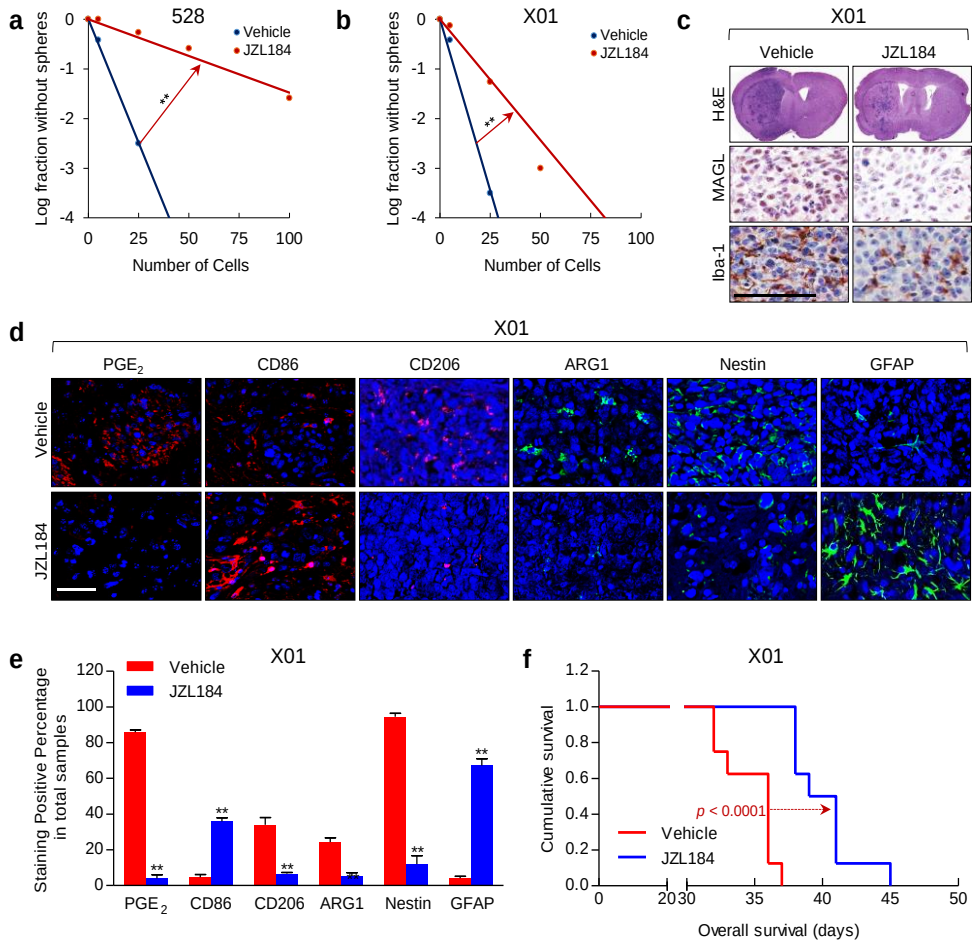

Figure 7. JZL184 Inhibits GSC Self-Renewal and Tumorigenicity

(A and B) Limiting dilution assays (LDAs) performed using 528 cells (B) and X01 cells (C) treated with JZL184 (1 μM).

(C) H&E staining of the whole brain and immunohistochemical (IHC) analysis of MAGL and Iba-1 in a JZL184-treated orthotopic xenograft mouse model. Scale bar, 100 μm. The sample is extracted at 32 days after

cell injection.

(D and E) Immunofluorescence (IF) analysis and quantification of PGE_2, CD86, CD206, ARG1, Nestin, and GFAP in a JZL184-treated orthotopic xenograft mouse model. Scale bar, 50 μm. Data are expressed as means ± SEM (error bars) (n = 3, ** P < 0.01).

(F) Kaplan-Meier survival analysis of mice implanted with X01 cells treated with JZL184 or vehicle (n = 8; 2.5×10^4 cells injected per mouse).

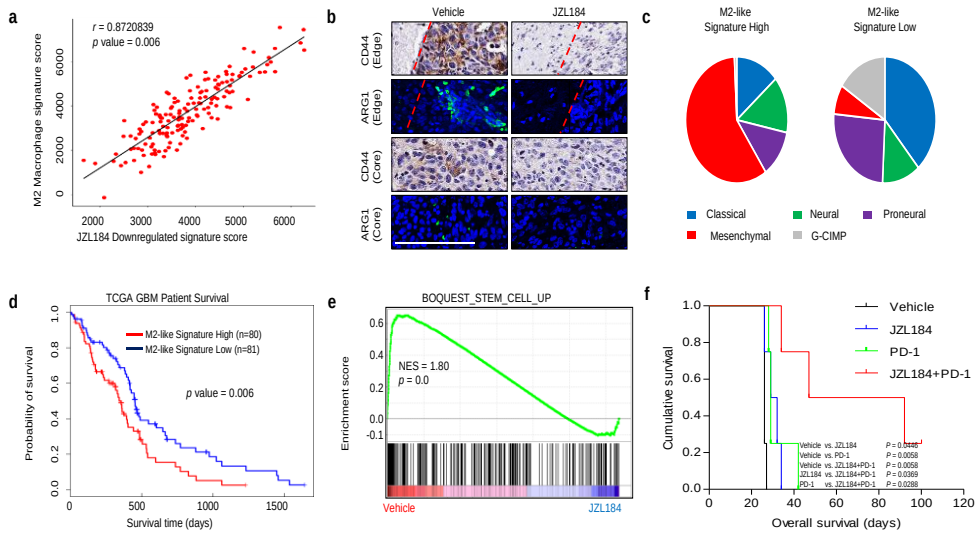

Figure 8. JZL184 Inhibits M2-like TAMs Signature and Associated with Patients Survival

(A) Correlation dot-plot of JZL184 downregulated gene signature and M2 gene signature of TAMs from vehicle vs. JZL184 treated subcutaneous mouse model.

(B) Immunohistochemical (IHC) and immunofluorescence (IF) analysis of CD44 and ARG1 in edge or core tumor regions of brain slices treated with JZL184 or vehicle. Scale bar, 100 μm.

(C) Pie chart of ratio of GBM subtypes according to high and low expression of M2-like gene signature.

(D) Kaplan-Meier survival plots for GBM patients in the TCGA data set according to high (top 50%) and low (bottom 50%) M2-like signature

expression.

(E) Gene Set Enrichment Analysis (GSEA) plot for stemness gene signature in comparison of TAMs from vehicle vs. JZL184 treated subcutaneous mouse model.

(F) GSEA plot for invasiveness gene signature in comparison of TAMs from vehicle vs. JZL184 treated subcutaneous mouse model.

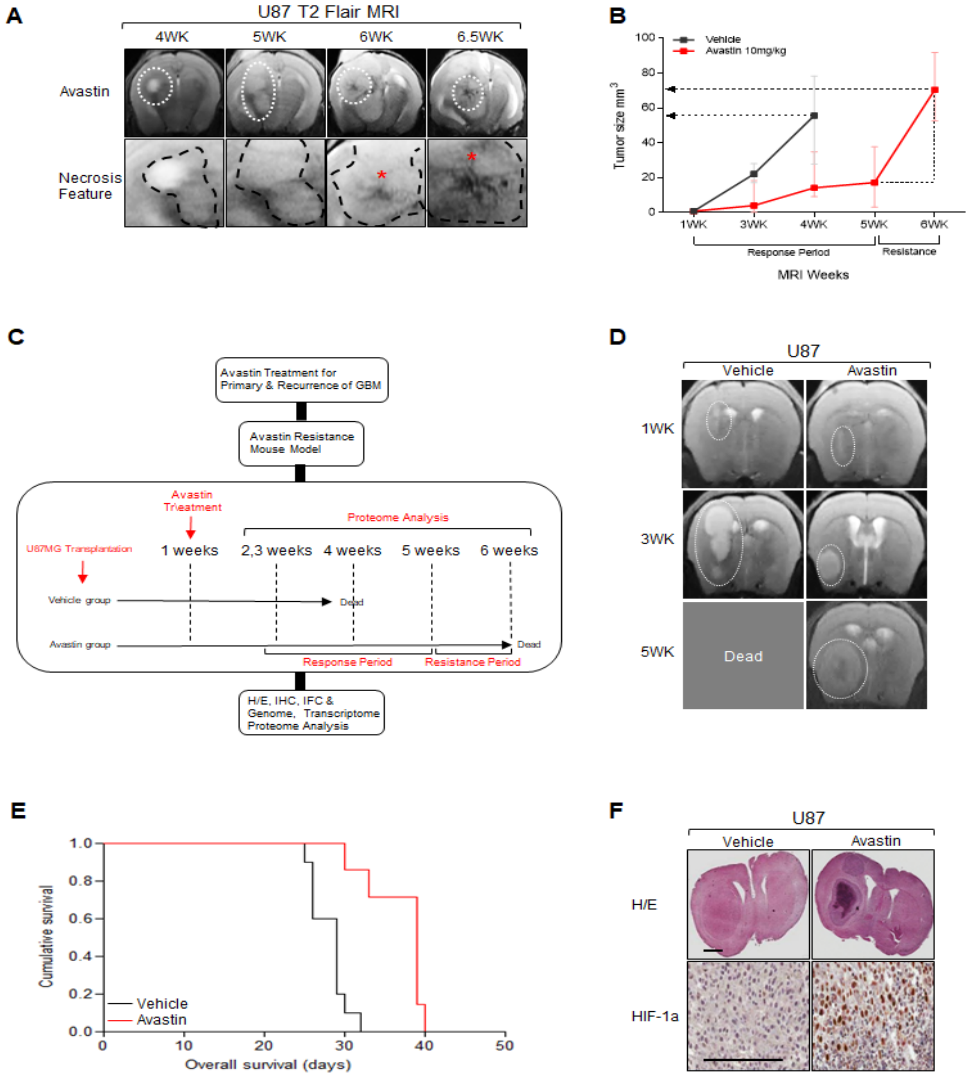

Fig. 9. Bevacizumab induced Resistance Model in U87MG. (A) Week-wise T2 Flair MRI follow-up in U87MG of brain orthotopic mouse model, Asteriks, necrosis regions. (B) Brain tumor size measuring graph from T2 Flair MRI images. (C) Schematic diagram of treating bevacizumab protocol after injecting U87MG. (D) U87MG injected mouse model with bevacizumab treatment follow-up by MRI. (E) Kaplan-Meier survival

analysis of mice implanted with U87MG cells (n = 7; 1×10^4 cells injected per mouse). Median survival of the orthotopic mice injected with vehicle or bevacizumab 32 days, 41 days, respectively. (F) H&E staining of the whole brains from mice implanted with U87MG cells injected with vehicle or bevacizumab. Scale bar, 100 μm.

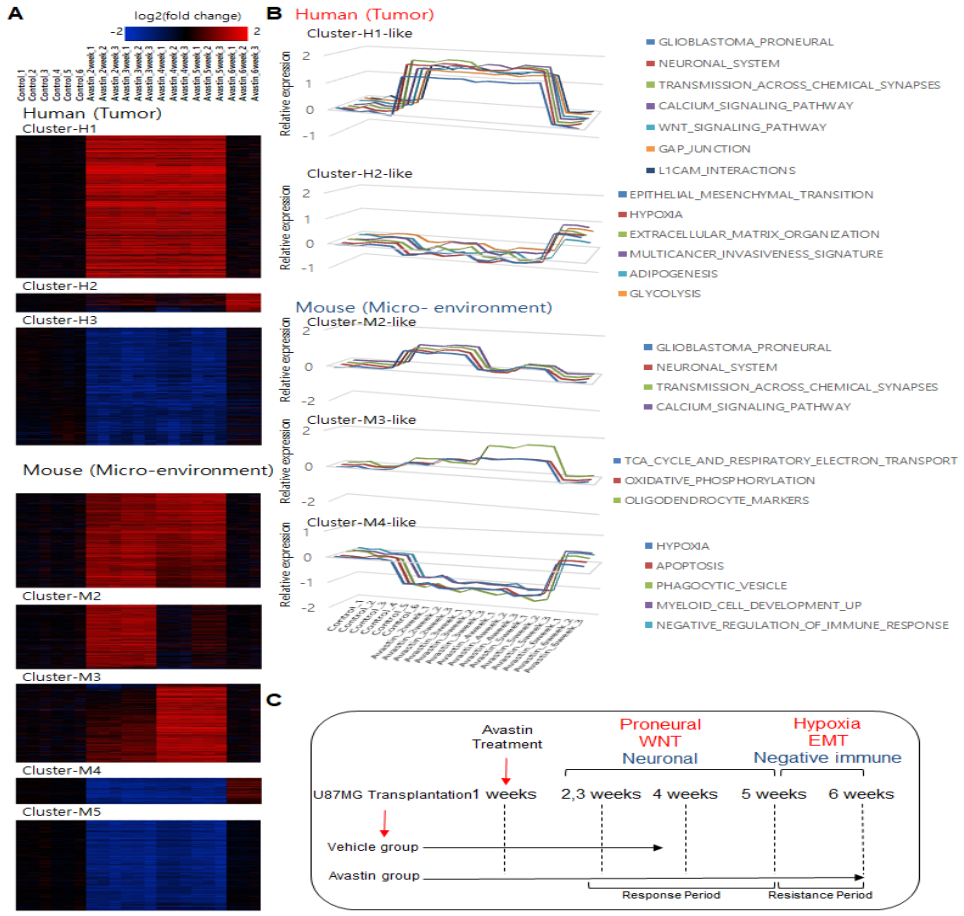

Fig. 10. Proteomic Landscape of Brain Tissue in Bevacizumab Murine Model. (A) Heatmap analysis of proteome analysis in U87MG brain tissues. (B) Week-wise sigmoid pattern of proteome signatures of U87MG brain tissues. (C) Schematic images of U87MG treatment of bevacizumab or vehicle.

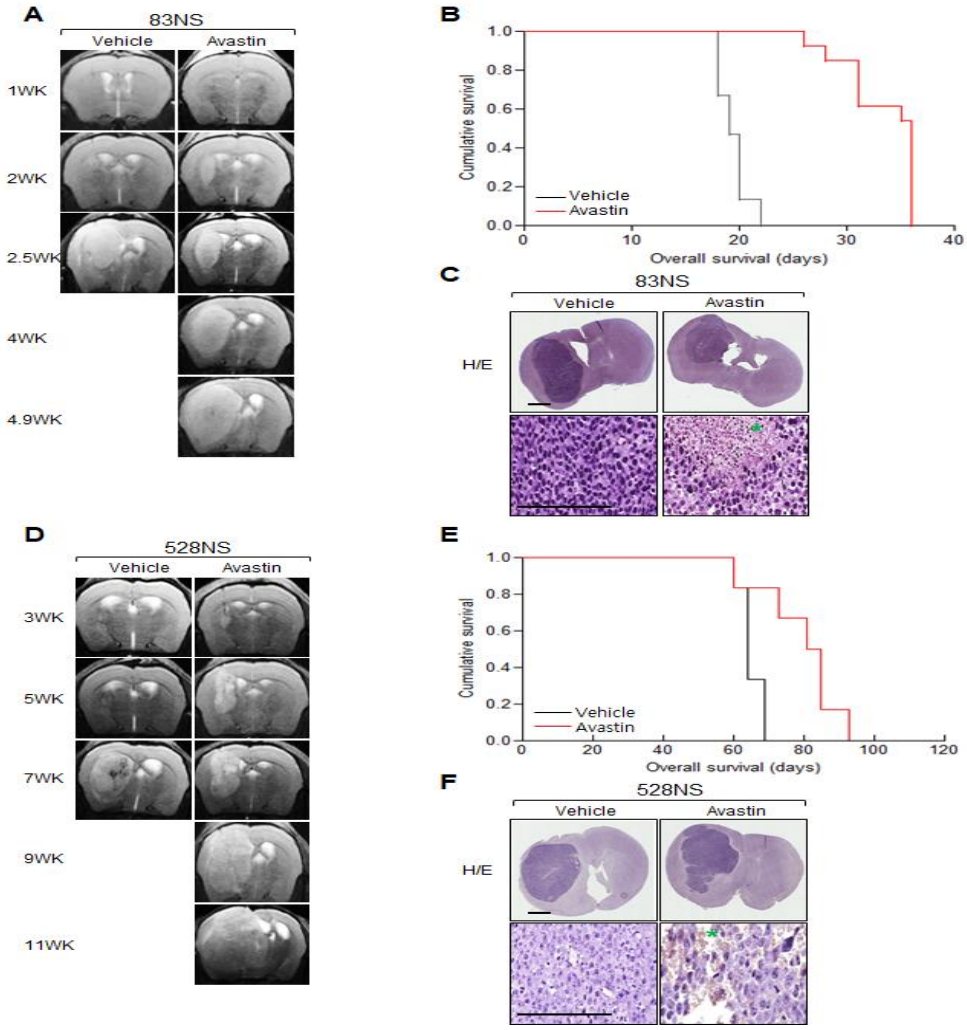

Fig. 11. Patient Derived GSCs have resistance mechanism against bevacizumab. (A and D) Week-wise T2 Flair MRI follow-up in 83NS and 528MS of brain orthotopic mouse model. (B – F) Kaplan-Meier survival analysis of mice implanted with 83NS and 528NS cells (n = 7; 1×10^4 cells injected per mouse). and H&E staining of the whole brains treated with vehicle or bevacizumab. Scale bar, 100 μm.

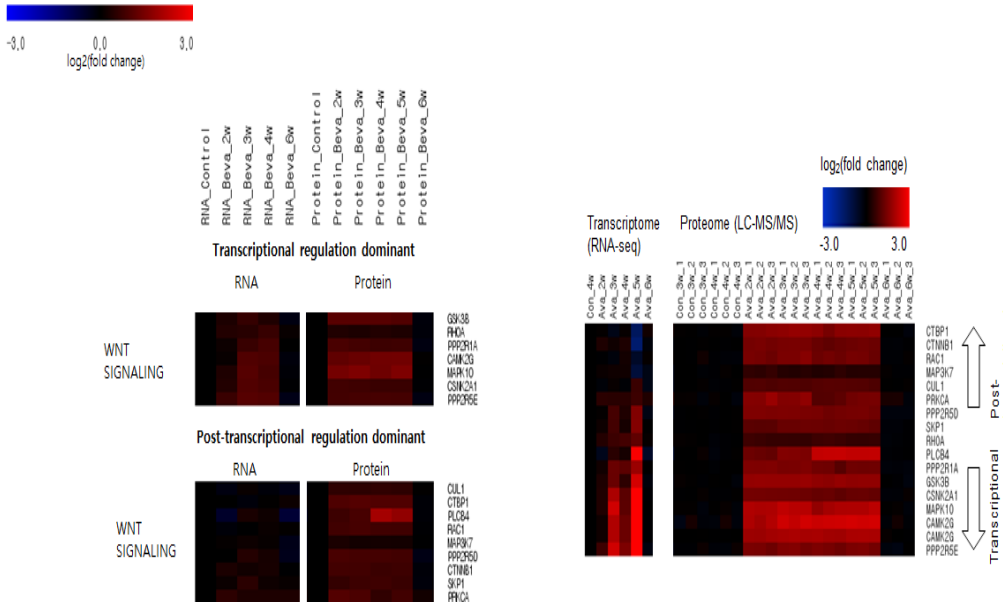

Fig. 12. Proteogenomic Analysis of WNT signaling for ß-Catenin expression. (A) Heatmap analysis of proteo-genome expression in U87MG cells for RNA sequencing and proteome results.

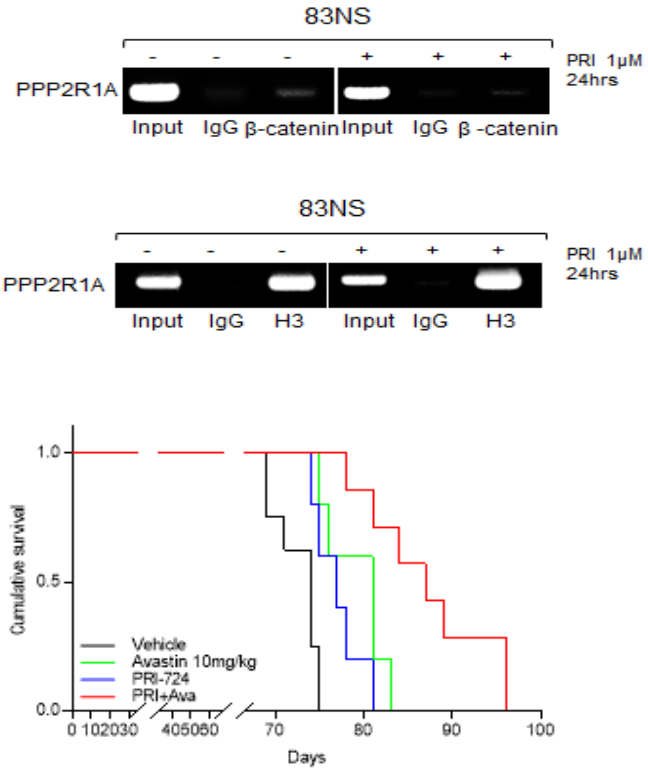

Fig. 13. Validated Down-signaling Axis of ß-Catenin by CHIP and *in vivo* model. Immunoprecipitated chromatin was analyzed by RT-PCR using specific primers on the promoter region of the ß-Catenin gene. And survival plot of PRI-724 combined with bevacizumab.

ACKNOWLEDGEMENT

I appreciate to your great supports, my doctoral degree thesis and all result were supported by Prof. Jong Bae Park for clinical scientific research. He accepted me as his pupil for researching brain tumor patient and its therapeutics. He didn't hesitate to advice and rebuke immature attitude of being a scientist. Also he generously gave me scientific knowledges as a professional of brain tumor for developing new therapeutics and elucidating mechanism of therapeutic resistance.
And I appreciate to my doctoral degree thesis committee members; Prof. Yun-Hee Kim, Prof. Jong Heon Kim, Prof. Yun Soo Bae and Prof. Myung Jin Park. They gave me encouraging advices to correct non-scientific points and welcome to my new research fields for elucidating therapeutic resistance. Prof. Yun-Hee Kim was chair for evaluating my doctoral degree thesis as a professional of pancreas cancer therapeutics. Prof. Jong Heon Kim gave me advice to correct non-scientific presentation data as a professional of RNA related cancer development. Prof. Yun Soo Bae evaluate my doctoral degree thesis for developing therapeutics as a professional for developing therapeutics from Ewha Univ. And Prof. Myung Jin Park gave me advice for MES transition as a professional about Cancer Stem Cell from KIRAMS
And I appreciate to my Lab. Members: Ph.D. Jinlong Yin, MD. Ph.D. Joon Hee Hong, Mr. Tae Hoon Kim, Mr. Saewhan Park, Mr. Hyung Joon Kwon, Ms. Yeonhee You, Ms. Weiwei Lin, Mr. Chan Il Kim, Ms. Ha Seo Ryu, Ms. So Yeon Jeon, Ms. Hey Ji Shin, Ms. Na Yeon Lee. Without theirs supports, I couldn't stand in National Cancer Center of South Korea as a translational scientist for brain cancer patient. Ph. D. Jinlong Yin and MD. Ph. D. Joon Hee Hong have me inspiration for developing immature idea for therapeutics. Dr. Tae Hoon Kim support me his ability for data analysis with dedicative attitude for developing therapeutics. Mr. Saewhan Park, Mr. Hyung Joon Kwon, Ms. Yeonhee You, Ms. Weiwei Lin, Mr. Chan Il Kim, Ms. Ha Seo Ryu, Ms. So Yeon Jeon, Ms. Hey Ji Shin, Ms. Na Yeon Lee support me with their full strength and truth heart for researches experiments.
I appreciate the dedicative supports for the youngest son of yours,
막내아들을 키워주신 김진해 아버지, 안정숙 어머니 어버이은혜 감사합니다. 모든 결과는 예수님께 영광이었으면 합니다. 어머니 보고 싶습니다. 두 분의 헌신적인 열정과 자식을 사랑하는 사랑이 저를 있게 하였습니다. 또한 두 분의 정직하고 성실한 모습을 배워 박사학위를 마무리 할 수 있었습니다.
And thanks to my family, I could finish doctoral degree course.
정원용, 김서영, 김흥수, 최정규, 김나영 감사합니다. 형제자매의 사랑 속에서 힘든 환경과 잃어버린 사랑을 극복할 수 있었습니다. 형제자매의 사랑이 있어서 또한 박사학위를 마무리 할 수 있었습니다.
I could stand in this world by your dedicative supports.

Sincerely. Your truly translational medicine scientist.